Cell



# Hypoxia and intra-complex genetic suppressors rescue complex I mutants by a shared mechanism

## Graphical abstract

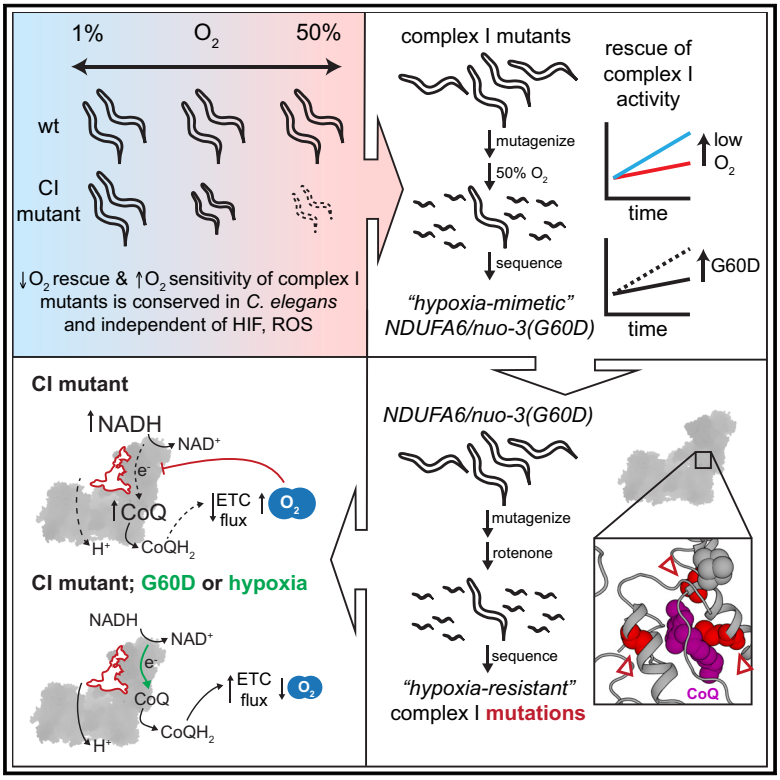


## Highlights

- Hypoxia rescue and hyperoxia sensitivity of complex I mutants are conserved in *C. elegans*
- Hypoxia rescue is independent of HIF activation or attenuation of ROS toxicity
- *NDUFA6/nuo-3(G60D)* mimics acute hypoxia in restoring complex I forward activity
- Residues in the CoQ binding pocket are required for rescue by *nuo-3(G60D)* or hypoxia


## Authors

Joshua D. Meisel, Maria Miranda, Owen S. Skinner, ..., Alexis A. Jourdain, Gary Ruvkun, Vamsi K. Mootha

## Correspondence

ruvkun@molbio.mgh.harvard.edu (G.R.), vamsi_mootha@hms.harvard.edu (V.K.M.)



## In brief

*C. elegans* mutants harboring a defective mitochondrial complex I are rescued by hypoxia or intra-complex genetic suppressor mutation, achieved by increasing forward flow of electrons through complex I and dependent on residues surrounding the CoQ binding pocket.


Meisel et al., 2024, Cell *187*, 1–17
February 1, 2024 
https://doi.org/10.1016/j.cell.2023.12.010

Cell

CellPress
OPEN ACCESS

Article

# Hypoxia and intra-complex genetic suppressors rescue complex I mutants by a shared mechanism

Joshua D. Meisel,[1,2,3,4] Maria Miranda,[1,2,3,4] Owen S. Skinner,[1,2,3,4] Presli P. Wiesenthal,[1,2] Sandra M. Wellner,[1,2,3,4,6] Alexis A. Jourdain,[1,2,3,4,7] Gary Ruvkun,[1,2,5,*] and Vamsi K. Mootha[1,2,3,4,5,8,*]

[1]Department of Molecular Biology, Massachusetts General Hospital, Boston, MA 02114, USA
[2]Harvard Medical School, Boston, MA 02115, USA
[3]Broad Institute, Cambridge, MA 02142, USA
[4]Howard Hughes Medical Institute, Massachusetts General Hospital, Boston, MA 02114, USA
[5]These authors contributed equally
[6]Present address: Department of Veterinary and Animal Sciences, University of Copenhagen, 1870 Frederiksberg, Denmark
[7]Present address: Department of Immunobiology, University of Lausanne, 1066 Epalinges, Switzerland
[8]Lead contact
*Correspondence: ruvkun@molbio.mgh.harvard.edu (G.R.), vamsi_mootha@hms.harvard.edu (V.K.M.)
https://doi.org/10.1016/j.cell.2023.12.010

## SUMMARY

The electron transport chain (ETC) of mitochondria, bacteria, and archaea couples electron flow to proton pumping and is adapted to diverse oxygen environments. Remarkably, in mice, neurological disease due to ETC complex I dysfunction is rescued by hypoxia through unknown mechanisms. Here, we show that hypoxia rescue and hyperoxia sensitivity of complex I deficiency are evolutionarily conserved to *C. elegans* and are specific to mutants that compromise the electron-conducting matrix arm. We show that hypoxia rescue does not involve the hypoxia-inducible factor pathway or attenuation of reactive oxygen species. To discover the mechanism, we use *C. elegans* genetic screens to identify suppressor mutations in the complex I accessory subunit *NDUFA6/nuo-3* that phenocopy hypoxia rescue. We show that *NDUFA6/nuo-3(G60D)* or hypoxia directly restores complex I forward activity, with downstream rescue of ETC flux and, in some cases, complex I levels. Additional screens identify residues within the ubiquinone binding pocket as being required for the rescue by *NDUFA6/nuo-3(G60D)* or hypoxia. This reveals oxygen-sensitive coupling between an accessory subunit and the quinone binding pocket of complex I that can restore forward activity in the same manner as hypoxia.

## INTRODUCTION

Complex I (NADH:ubiquinone oxidoreductase or CI) is the primary entry point of electrons into the ETC, using NADH to reduce flavin and iron-sulfur clusters in proteins along a path to ubiquinone (CoQ) and harnessing this electromotive force to pump protons across the mitochondrial inner membrane.[1,2] Complex I consists of 14 core subunits evolutionarily conserved from bacteria to mammals as well as dozens of accessory (or "supernumerary") subunits that perform structural and/or regulatory roles, organized into functional modules (N, Q, $P_P$, and $P_d$) corresponding to assembly intermediates.[3,4] Loss of complex I activity has numerous consequences for the cell, including decreased ATP production, loss of mitochondrial membrane potential, increased NADH/$NAD^+$ ratio, and accumulation of excess, unused molecular oxygen. Deficiencies in complex I of the ETC underlie approximately 30% of mitochondrial diseases, including Leigh syndrome, Leber's hereditary optic neuropathy, and MELAS—devastating human disorders for which there are no approved medicines.[5–7] Loss of complex I activity is also associated with more common forms of neurodegeneration and even certain rare cancers.[8–10]

A mouse model of Leigh syndrome caused by homozygous deletion of the complex I subunit *Ndufs4* is rescued by environmental hypoxia (11% oxygen), which extends lifespan, prevents neurodegeneration, and reverses late-stage neurological disease.[11,12] Conversely, exposure of the *Ndufs4* knockout mouse to moderate hyperoxia (55% oxygen) exacerbates the disease, causing rapid death. *Ndufs4* mice experience tissue hyperoxia in the brain at 21% oxygen, presumably due to decreased oxygen consumption by the ETC, and interventions that lower brain oxygen levels rescue neurological disease and extend lifespan.[13] These findings indicate that oxygen is central to the neuropathology, but the precise mechanism underlying the complex I rescue by hypoxia and sensitivity to hyperoxia has not been established. Moreover, whether these phenomena are evolutionarily conserved and translate to other *in vivo* models of complex I deficiency is unknown.

*Caenorhabditis elegans* is an ideal system to dissect the genetic-environmental interaction of complex I dysfunction and

Please cite this article in press as: Meisel et al., Hypoxia and intra-complex genetic suppressors rescue complex I mutants by a shared mechanism, Cell (2024), https://doi.org/10.1016/j.cell.2023.12.010



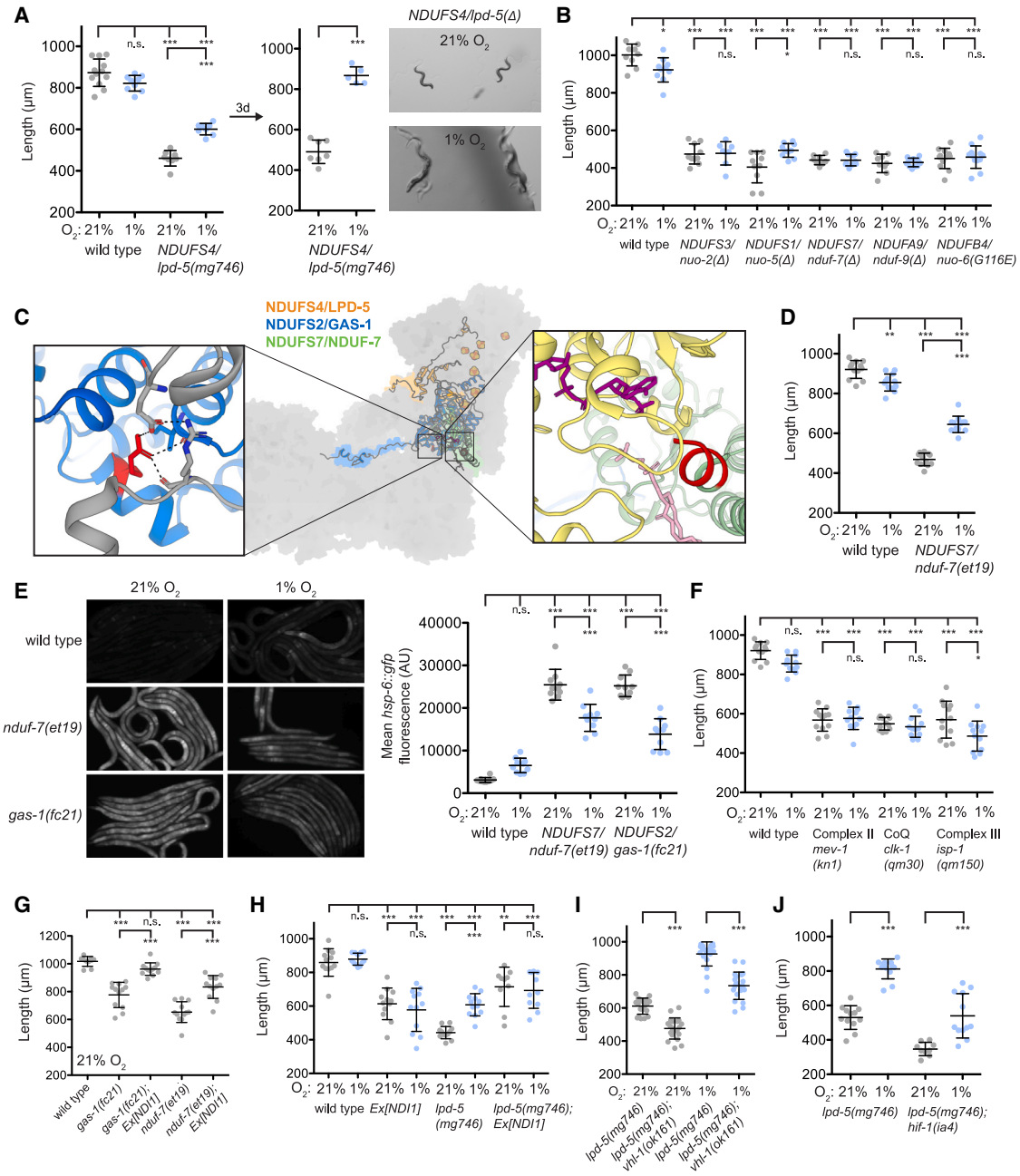


**Figure 1. A subset of complex I mutations are rescued by hypoxia independent of HIF**

(A) Growth of animals for 2 days (left) and 5 days (right) at 21% or 1% oxygen at room temperature.

(B) Growth of wild-type and *nuo-6(qm200)* animals for 2 days; growth of *nuo-2(tm5258)*, *nuo-5(tm2751)*, *nduf-7(tm1436)*, and *nduf-9(mg747)* animals for 4 days at room temperature.

(C) Ovine NADH:ubiquinone oxidoreductase, or complex I (PDB: 6ZKC[25]) in closed conformation. Colored red (on right) are the 6 homologous C-terminal amino acids deleted in *NDUFS7/nduf-7(et19)* that interact with NDUFA9/NDUF-9 (yellow), phospholipid headgroups (pink), and NADPH (purple). Colored red (on left) is NDUFS2/GAS-1(R290) which is substituted to K in *NDUFS2/gas-1(fc21)* and interacts with conserved residues E200 and R260 of ND1/NDUO-1 (gray). All NDUFS4/LPD-5 (orange) is lost in *lpd-5(mg746)*.

(D) Growth of animals for 2 days at room temperature.

(E) Fluorescent images of age-matched L4 stage animals containing *hsp-6::gfp* grown at 21% or 1% oxygen for one generation (left). Images were acquired at 69× magnification with an exposure time of 100 ms. Mean intestinal fluorescence of *hsp-6::gfp* in pictured animals (right).

(F) Growth of wild-type, *mev-1(kn1)*, and *clk-1(qm30)* animals for 2 days; growth of *isp-1(qm150)* animals for 3 days. The same wild-type controls are used in (D) as the data were collected in the same experiment.

*(legend continued on next page)*

oxygen. Nematode and mammalian complex I are highly homologous, with at least 42 of the 45 mammalian complex I subunits conserved.[14] Years of *C. elegans* genetic analysis of energy metabolism, anesthetic sensitivity, statin resistance, and longevity have generated a collection of viable complex I mutants.[15–18] *C. elegans* is commonly isolated from rotting fruit and vegetation on which abundant and diverse oxygen-consuming bacteria flourish.[19] Wild-type *C. elegans* prefer oxygen levels of 7%–8%,[20] perhaps because hypoxia is correlated with bacterial nutrition. However, *C. elegans* are naturally tolerant of a wide range of oxygen tensions, capable of reproducing and maintaining their metabolic rate from 1% to 100% oxygen.[21] Some *C. elegans* mitochondrial mutants are hypersensitive to elevated oxygen levels,[22–24] consistent with the *Ndufs4* mutant mouse findings.

Here, we show that hypoxia rescue of complex I deficiency is evolutionarily conserved to *C. elegans* and report that only a subset of complex I mutations are rescued by hypoxia and sensitive to moderate hyperoxia. These mutations partially compromise the soluble matrix arm of complex I (N and Q modules) that normally transfers electrons from NADH to CoQ. The rescue by hypoxia is neither dependent on the canonical oxygen-sensing hypoxia-inducible factor (HIF) signaling pathway, nor does attenuation of mitochondrial reactive oxygen species (ROS) toxicity underlie the rescue by hypoxia or sensitivity to hyperoxia. Using *C. elegans* forward genetic selections, we identify intra-complex amino acid substitution mutations in accessory subunits *NDUFA6/nuo-3* and *NDUFA5/ndua-5* that phenocopy the suppression of complex I mutants by hypoxia. Through biochemical studies, we show that *NDUFA6/nuo-3(G60D)* or hypoxia partially restore complex I forward electron transport activity, with downstream rescue of ETC flux and, in some cases, complex I levels. Additional *C. elegans* genetic screens identify NDUFS7/NDUF-7 and NDUFS2/GAS-1 amino acid residues surrounding the ubiquinone binding pocket that are necessary for the rescue of complex I mutants by *NDUFA6/nuo-3(G60D)* or hypoxia. These results suggest that mutants harboring a defective complex I are rescued by increasing forward flow of electrons to CoQ, achieved through structural changes in the CoQ binding pocket.

## RESULTS

### Hypoxia rescues a subset of complex I mutations in *C. elegans*

To determine if *C. elegans* ETC mutants are rescued by hypoxia, we exposed wild-type or mutant L1 stage animals to 21% or 1% oxygen and measured their rate of growth and development. *C. elegans* homozygous for a deletion in *NDUFS4/lpd-5* encoding a supernumerary subunit of complex I arrested development in normoxia at an early larval stage, but animals at 1% oxygen developed beyond this arrest point to sterile adulthood (Figure 1A). This is consistent with hypoxia rescue of the mouse *Ndufs4* knockout. However, complete loss of complex I activity cannot be rescued by hypoxia, as deletions in subunits *NDUFS3/nuo-2*, *NDUFS1/nuo-5*, *NDUFS7/nduf-7*, or *NDUFA9/nduf-9* caused early developmental arrest at 21% oxygen with no improvement at 1% oxygen (Figure 1B). Chemical inhibition of complex I activity with the plant natural product rotenone also caused developmental delay that was not rescued by hypoxia (Figure S1A). These results demonstrate that rescue of particular complex I deficiencies by hypoxia is evolutionarily conserved but does not generalize to all complex I lesions.

To further understand which complex I mutants are amenable to rescue by hypoxia, we tested additional mutations in the electron-conducting matrix arm. Animals carrying a partial loss-of-function allele in the complex I core subunit *NDUFS7/nduf-7(et19)* are viable, have reduced complex I activity, and grow slowly at 21% oxygen.[18] The *NDUFS7/nduf-7(et19)* mutation eliminates the last 6 amino acids of NDUF-7 which lie on the surface of complex I and are likely to stabilize interactions with the supernumerary subunit NDUFA9/NDUF-9, phospholipid headgroups, and non-catalytic NADPH (Figures 1C and S1B). In contrast to an *nduf-7* deletion allele, the *nduf-7(et19)* mutant is partially rescued by hypoxia, growing faster at 1% oxygen (Figure 1D). Expression of the mitochondrial stress reporter *hsp-6::gfp*—a fusion to the promoter of an HSP70 mitochondrial chaperone and readout of mitochondrial membrane potential and protein import efficiency[26,27]—was elevated in *nduf-7(et19)* animals grown at 21% oxygen but attenuated in animals grown at 1% oxygen, suggesting that hypoxia restores mitochondrial function (Figure 1E). Another hypomorphic mutation in the complex I Q module, *NDUFS2/gas-1(fc21)*, is an R290K substitution that causes reduced complex I activity, hypersensitivity to volatile anesthetics, and low broodsize.[15,16] NDUFS2/GAS-1(R290) is a highly conserved residue that may form stabilizing interactions with the mitochondrial-genome-encoded membrane subunit ND1 (Figures 1C and S1B). Although hypoxia did not significantly rescue *gas-1(fc21)* growth rate (data not shown), possibly due to a mild phenotype at 21% oxygen, *gas-1(fc21)* strongly induced *hsp-6::gfp* at 21% oxygen, and this induction was decreased in 1% oxygen (Figures 1E and S1C), suggesting that the *gas-1(fc21)* complex I mutant is also partially rescued by hypoxia.

We tested if the slow growth of complex I mutants in the proton-pumping membrane arm was also suppressed by hypoxia. A partial loss-of-function allele of the membrane supernumerary subunit *NDUFB4/nuo-6(qm200)* with low complex I activity[17] did not grow faster at 1% oxygen (Figure 1B). *nuo-6(qm200)* also induced *hsp-6::gfp* expression and this was not altered by 1% oxygen, further suggesting that this mutant is not rescued by hypoxia (Figure S1C). This also demonstrates that the *hsp-6::gfp* reporter is not basally affected by 1% oxygen independent of complex I, consistent with decreased *hsp-6::gfp* fluorescence in *gas-1(fc21)* and *nduf-7(et19)* animals exposed to hypoxia reflecting increased complex I activity. Similarly, *hsp-6::gfp* levels were elevated in *NDUFS4/lpd-5(mg746)* and *NDUFS3/nuo-2(tm5258)* null mutants but partially suppressed by hypoxia

(G) Growth of animals for 3 days at 20°C.
(H–J) Growth of animals for 2 days (H), 5 days (I), or for 4 days (J) at room temperature. Statistical significance was calculated using one-way ANOVA followed by Tukey's multiple comparison test. Error bars represent standard deviation. n.s., not significant, *p value < 0.05, **p value < 0.01, ***p value < 0.001.
See also Figure S1 and Table S1.

Please cite this article in press as: Meisel et al., Hypoxia and intra-complex genetic suppressors rescue complex I mutants by a shared mechanism, Cell (2024), https://doi.org/10.1016/j.cell.2023.12.010



only in *lpd-5(mg746)* (Figure S1C). Viable, slow-growing *C. elegans* mutants in other components of the ETC including *mev-1(kn1)*/complex II, *clk-1(qm30)*/CoQ biosynthesis, and *isp-1(qm150)*/complex III also exhibited a growth delay that was not rescued by hypoxia (Figure 1F). Taken together, these results indicate that a subset of complex I mutants can be rescued by hypoxia—specifically those that partially compromise the soluble portion (N and Q modules) of complex I responsible for passing electrons from NADH to CoQ (Table S1).

A set of fungal species that includes *S. cerevisiae* have lost the multisubunit, proton-pumping complex I and instead harbor NDI1, a mitochondrial inner membrane type II NADH dehydrogenase.[28] This single polypeptide catalyzes two-electron transfer from NADH to CoQ without pumping protons and can rescue the survival and growth defects of complex I mutant mammals or *C. elegans*.[29–31] Expression of yeast NDI1 rescued the slow growth of *lpd-5(mg746)*, *nduf-7(et19)*, and *gas-1(fc21)* mutant *C. elegans* at 21% oxygen (Figures 1G and 1H). NDI1 could also suppress the growth arrest of complex I mutants *nduf-9(mg747)* and *nuo-6(qm200)* which were not rescued by hypoxia, demonstrating that their growth defect is indeed due to complex I deficiency (Figure S1D). Interestingly, although hypoxia improved the growth of *lpd-5(mg746)* and *nduf-7(et19)* mutants, it did not further benefit these complex I mutants when NDI1 was expressed despite a dynamic range sufficient for additivity (Figures 1H and S1E). This is consistent with NDI1 activity covering the same specific defect rescued by hypoxia (i.e., passing electrons from NADH to CoQ); alternatively, hypoxia may have no effect in these genetic backgrounds due to NDI1-expressing animals having a liability in hypoxia.

## Hypoxia rescue of *C. elegans* complex I mutants is independent of the HIF transcriptional response

To determine if hypoxia rescues through the canonical HIF transcription factor-mediated oxygen-sensing pathway, we constructed double mutants with complex I subunits and components of the HIF signaling pathway. VHL-1 is an E3 ubiquitin ligase that targets EGLN-mediated hydroxylated HIF for degradation.[32] VHL-1 null mutants constitutively activate the hypoxia response even at normoxia. Neither *lpd-5(mg746)* nor *nduf-7(et19)*—mutants whose growth is rescued by hypoxia—were improved by loss of *vhl-1* at 21% oxygen (Figures 1I and S1F). In fact, the *nduf-7; vhl-1* and *lpd-5; vhl-1* double mutants grew more slowly than the complex I single mutants. This is consistent with observations in the *Ndufs4* mouse[13] and suggests activation of the HIF hypoxia response is not sufficient to rescue the slow growth of complex I mutants. We wondered if activation of HIF may be beneficial in the context of hypoxia, where its response is physiologically adaptive, but at 1% oxygen VHL-1 loss was also detrimental to the *lpd-5* and *nduf-7* mutants (Figures 1I and S1F). *C. elegans* contains only one HIF homolog, HIF-1, and HIF-1 null mutants are viable. This allowed us to ask if the HIF hypoxia response was necessary for the rescue by hypoxia. Despite *hif-1* mutants themselves being sensitive to hypoxia, the *nduf-7; hif-1* and *lpd-5; hif-1* double mutants were both partially rescued by 1% oxygen (Figures 1J and S1G), demonstrating that the HIF transcriptional response to hypoxia is not necessary for the hypoxia rescue of complex I mutants.

## Complex I mutants rescued by hypoxia are also sensitive to 50% oxygen

To further characterize the interaction between complex I deficiency and oxygen tension, we exposed viable, slow-growing ETC mutants to 50% and 100% oxygen (hyperoxia). Multiple *C. elegans* mitochondrial mutants were sensitive to 100% oxygen, including mutants in complex I, complex II, CoQ biosynthesis, and complex III (Figures 2A and S2A), as observed previously.[22–24] 100% oxygen also caused wild-type animals to develop slowly and induced the *hsp-6::gfp* mitochondrial stress reporter, indicating mitochondrial dysfunction (Figures 2A, 2B, and S2A). However, at 50% oxygen, the growth of wild-type animals was not delayed, the *hsp-6::gfp* mitochondrial stress reporter was not induced, and ETC mutants in complex II, CoQ biosynthesis, and complex III were able to develop to fertile adulthood (Figures 2A, 2B, and S2A). The only viable mutants that arrested development at 50% oxygen were the complex I mutants *NDUFS7*/*nduf-7(et19)* and *NDUFS2*/*gas-1(fc21)*, which arrested at the L1 stage and L2 stage, respectively (Figure 2A). *nduf-7(et19)* and *gas-1(fc21)* mutants recovered from at least 6 days exposure to 50% oxygen when shifted to 21% oxygen (Figure S2B), suggestive of a reversible developmental arrest and reminiscent of the ability of advanced brain disease in *Ndufs4* knockout mice to be reversed by hypoxia.[12] The sensitivity of *nduf-7(et19)* and *gas-1(fc21)* to 50% oxygen was rescued by expression of yeast NDI1 (Figure S2C), indicating that the vulnerability to hyperoxia arises from impairment of complex I oxidation of NADH or reduction of ubiquinone. Notably, the slow-growing complex I mutant NDUFB4/*nuo-6(qm200)*, which was not rescued by hypoxia, is also not sensitive to hyperoxia (Figure S2A). Taken together, these results suggest a mechanistic link between growth rescue by hypoxia and sensitivity to moderate hyperoxia (Table S1).

## Oxygen-sensitive complex I mutants are suppressed by intra-complex mutations in *NDUFA6* and *NDUFA5*

Based on these *C. elegans* genetic results and the extreme sensitivity to moderate hyperoxia of the *Ndufs4* mouse,[11] we sought to identify *C. elegans* genetic suppressor mutations of the hyperoxia sensitivity in complex I mutants. To isolate such mutations, we performed two parallel forward genetic screens for suppressors of the *nduf-7(et19)* or *gas-1(fc21)* growth arrest at 50% oxygen. *C. elegans* animals were mutagenized with a DNA alkylating agent and grown at 21% oxygen for two generations to generate hundreds of thousands of randomly distributed new mutant alleles for genetic selection. This large collection of F2 generation animals was transferred to the non-permissive 50% oxygen tension as synchronized L1 animals and screened for rare mutants that could grow to adulthood. The nuclear and mitochondrial genomes of these suppressor mutants were then deep-sequenced (Figure 2C). As an endorsement of the depth of the selection, each of these screens identified intragenic amino acid substitutions in *nduf-7* or *gas-1* that acted as revertants of the original *nduf-7(et19)* or *gas-1(fc21)* mutations (Table S2). More importantly, the screens identified three independent dominant alleles of the complex I subunit *NDUFA6*/*nuo-3*, all of which encode G60D missense mutations, and one allele in the complex I subunit *NDUFA5*/*ndua-5* that encodes

Please cite this article in press as: Meisel et al., Hypoxia and intra-complex genetic suppressors rescue complex I mutants by a shared mechanism, Cell (2024), https://doi.org/10.1016/j.cell.2023.12.010



CellPress
OPEN ACCESS

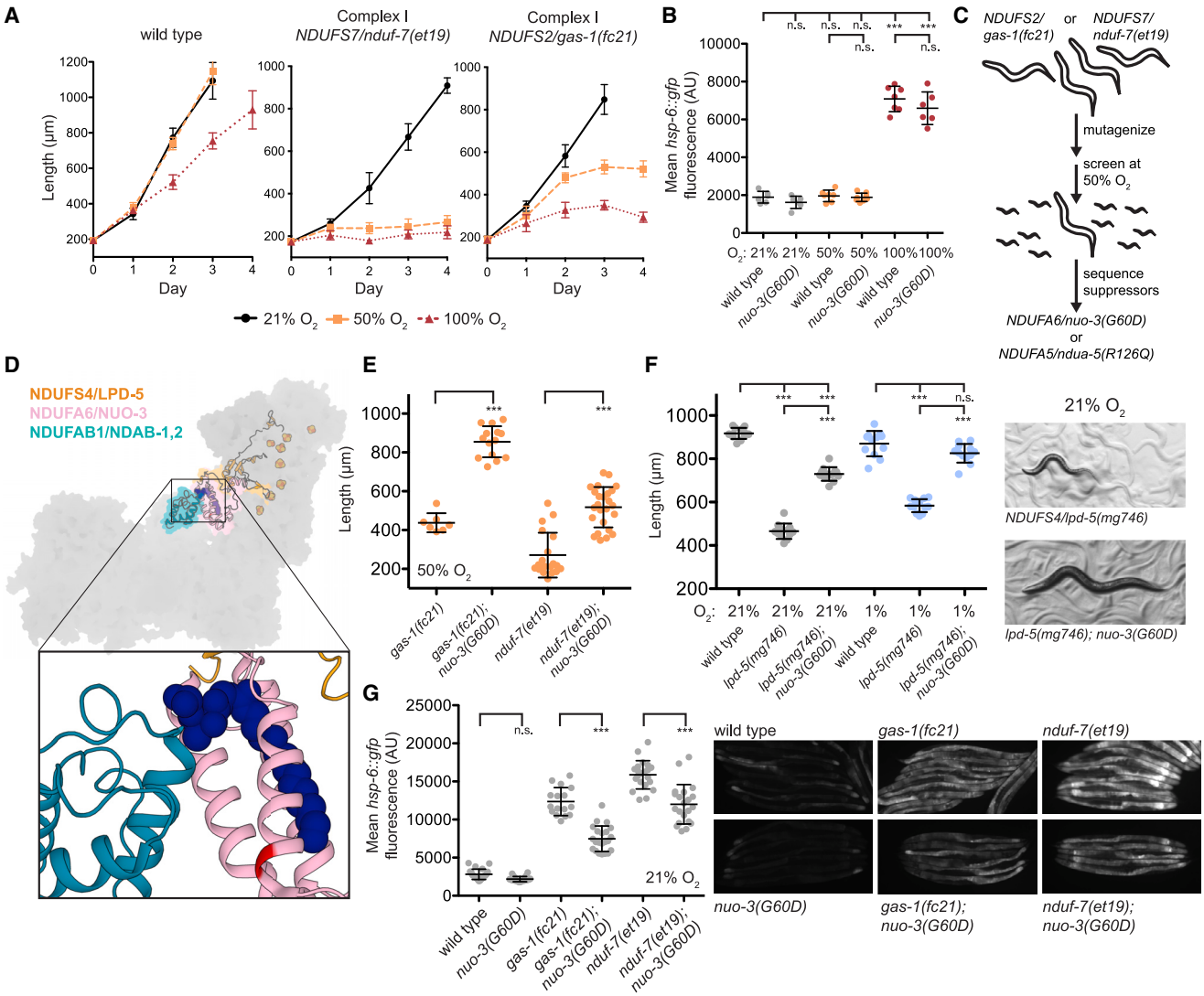


**Figure 2. Complex I mutants rescued by hypoxia are sensitive to moderate hyperoxia and suppressed by intra-complex mutations in *NDUFA6* or *NDUFA5***

(A) Growth of animals following L1 synchronization at 21% oxygen (black), 50% oxygen (orange), or 100% oxygen (red) incubated at 20°C.

(B) Mean intestinal fluorescence of *hsp-6::gfp* in L4 stage animals incubated at 21%, 50%, or 100% oxygen for 1 day at 20°C. Exposure time = 100 ms, magnification = 69×.

(C) *gas-1(fc21)* or *nduf-7(et19)* P0 animals were randomly mutagenized with ethyl methanesulfonate (EMS) at 21% oxygen. F2 progeny were transferred to the non-permissive 50% oxygen tension and selected for growth. NDUFS4/*lpd-5* null *C. elegans* are not fertile at any oxygen tension, making a forward genetic screen challenging.

(D) Ovine complex I (PDB: 6ZKC[25]) in closed conformation. Colored red is the ovine residue (K57) corresponding to *C. elegans* suppressor mutation *NDUFA6/nuo-3(G60D)* which lies in the LYRM domain responsible for binding the acyl chain (purple) of NDUFAB1.

(E) Growth of animals for 4 days at 50% oxygen followed by 1 day at 21% oxygen.

(F) Growth of animals for 2 days (graph, left) and 4 days (images, right) at room temperature.

(G) Mean intestinal fluorescence of *hsp-6::gfp* in L4 stage animals incubated at continuous 21% oxygen at 20°C. For all panels, statistical significance was calculated using one-way ANOVA followed by Tukey's multiple comparison test. Error bars represent standard deviation. n.s., not significant, *p value < 0.05, **p value < 0.01, ***p value < 0.001.

See also Figure S2 and Table S2.

an R126Q missense mutation (Table S2). The *nuo-3(G60D)* and *ndua-5(R126Q)* intra-complex suppressors lie in accessory subunits on opposite sides of the interface between the matrix and membrane domains of complex I (Figures 2D and S2D).

To prove that these candidate lesions caused the suppression of hyperoxia arrest, we used CRISPR-Cas9 to generate a *nuo-3(G60D)* allele in a wild-type genetic background and then introduced this mutation into complex I mutants. The

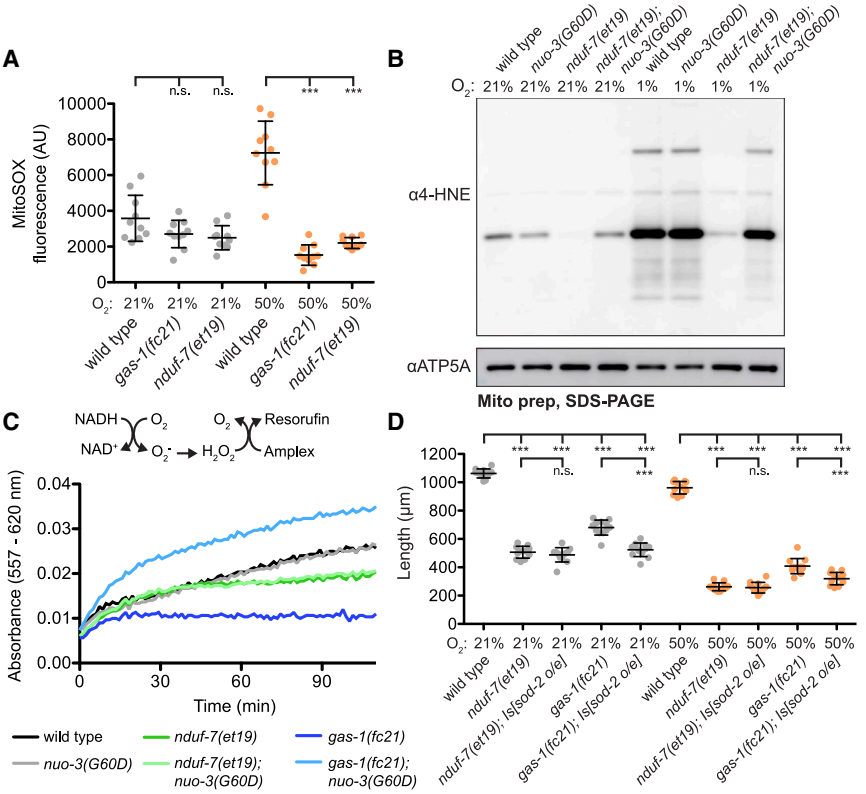


**Figure 3. Rescue of complex I mutants by hypoxia and *nuo-3(G60D)* is not due to alleviation of mitochondrial ROS**

(A) MitoSOX fluorescence quantified by measuring the mean fluorescence in the posterior bulb of the pharynx after 1 day. Images were taken with an exposure time of 1 second at 63× magnification.

(B) SDS-PAGE western blot of isolated mitochondria purified from animals grown at 21% or 1% oxygen for 4 days. The mitochondrial proteins modified by 4-HNE in this experiment are unidentified.

(C) NADH-driven complex I-dependent superoxide production in the absence of piericidin by isolated mitochondrial membranes at 21% oxygen. Superoxide is converted by SOD to hydrogen peroxide, which then oxidizes AmplexRed to resorufin via horseradish peroxidase (HRP). Resorufin absorbs light at 557 nm.

(D) Growth of animals for 2 days at room temperature at 21% or 50% oxygen. For all panels, statistical significance was calculated using one-way ANOVA followed by Tukey's multiple comparison test. Error bars represent standard deviation. n.s., not significant, *p value < 0.05, **p value < 0.01, ***p value < 0.001.

See also Figure S3.

CRISPR-generated *nuo-3(G60D)* allele suppressed the *nduf-7(et19)* and *gas-1(fc21)* sensitivity to hyperoxia, confirming *nuo-3(G60D)* as the causative mutation in our screen (Figure 2E). We also found that *nuo-3(G60D)* is an excellent suppressor of the *NDUFS4/lpd-5* null mutant, allowing the animals to develop to sterile adulthood at 21% oxygen much like the rescue by hypoxia (Figure 2F). Consistent with *nuo-3(G60D)* acting dominantly, the effects of hypoxia and *nuo-3(G60D)* on the *NDUFS4/lpd-5(mg746)* mutant were additive with respect to growth rate (Figure 2F), and more strikingly, the *lpd-5(mg746); nuo-3(G60D)* double mutant in 1% oxygen was a non-sterile and viable strain able to generate progeny (Figure S2E). A similar CRISPR-based approach confirmed *NDUFA5/ndua-5(R126Q)* as a genuine complex I suppressor of *nduf-7(et19)* and *gas-1(fc21)* at 50% oxygen, and *lpd-5(mg746)* at 21% and 1% oxygen (Figures S2F–S2H). These results show that mutations in two distinct complex I genes can each suppress three distinct complex I lesions, suggesting they exert a general protective effect on complex I. We focus on the *nuo-3(G60D)* mutation that conferred the stronger suppression phenotype for the remainder of this study.

*nuo-3(G60D)* caused a partial reduction of *hsp-6::gfp* induction in the *nduf-7(et19)* and *gas-1(fc21)* mutants, suggesting an alleviation of mitochondrial stress through restored ETC activity (Figure 2G). Notably, *nuo-3(G60D)* did not reduce *hsp-6::gfp* expression in wild-type animals exposed to 100% oxygen, arguing against a protective effect on oxygen toxicity more broadly and pointing to suppression of specific complex I mutants (Figure 2B). Although *nuo-3(G60D)* was able to suppress *nduf-7(et19), gas-1(fc21)*, and *lpd-5(mg746)* animals, *nuo-3(G60D)* did not suppress other complex I mutants such as *NDUFA9/nduf-9(mg747)* and *NDUFB4/nuo-6(qm200)* at any oxygen tension (Figures S2I and S2J). *nuo-3(G60D)* also did not suppress slow-growing ETC mutants in complex II, CoQ biosynthesis, and complex III at any oxygen tension (Figure S2K). The emerging pattern is that the genetic requirements for rescue by 1% oxygen, sensitivity to 50% oxygen, and rescue by *nuo-3(G60D)* are identical, and we hypothesize that common mechanisms underlie these phenomena (Table S1).

## Mitochondrial ROS toxicity does not underlie the mutant rescue by hypoxia or *nuo-3(G60D)*

Excess molecular oxygen can undergo partial reduction to form ROS (e.g., superoxide, hydrogen peroxide), and *C. elegans* mitochondrial mutants are sensitive to exogenous canonical forms of oxidative stress.[23,33] Therefore, we measured steady-state levels of mitochondrial ROS in our mutants using MitoSOX, a dye targeted to the mitochondria that is oxidized by superoxide to produce red fluorescence. *gas-1(fc21)* and *nduf-7(et19)* displayed wild-type or decreased MitoSOX staining at 21% and 50% oxygen (Figure 3A), consistent with prior reports.[34,35] However, because mitochondrial uptake of MitoSOX is dependent on mitochondrial membrane potential, which is compromised in complex I mutants, we sought to validate this finding with orthogonal approaches. First, we analyzed expression of *gst-4::gfp*, a reporter for the NRF2-mediated antioxidant response, and found that its expression was not activated in the *nduf-7(et19)* and *gas-1(fc21)* mutants (Figure S3A). Exposure to 100% oxygen did activate the *gst-4::gfp* reporter in wild type, but induction in the complex I mutant

backgrounds was comparable. Second, we isolated mitochondria and performed western blots with an antibody against 4-hydroxynonenal (4-HNE), a product of lipid peroxidation that can bond covalently to lysine residues through Schiff base formation.[36] Consistent with the MitoSOX results, *nduf-7(et19)* displayed dramatically decreased 4-HNE staining, which was normalized by *nuo-3(G60D)* at both 21% and 1% oxygen (Figure 3B). Third, we directly measured ROS produced from complex I in purified mitochondrial membranes. In this *in vitro* assay, NADH-driven superoxide production from complex I is converted to hydrogen peroxide, which is used to oxidize Amplex Red. Both *nduf-7(et19)* and *gas-1(fc21)* displayed decreased ROS production by complex I, and *nuo-3(G60D)* increased ROS production in the *gas-1(fc21)* background (Figure 3C). Finally, we introduced transgenes over-expressing mitochondrial-localized superoxide dismutase (SOD) SOD-2, which detoxifies superoxide into hydrogen peroxide, and observed no rescue of *nduf-7(et19)* or *gas-1(fc21)* slow growth rate at 21% or 50% oxygen (Figure 3D). Over-expression of SOD-2 in combination with mitochondrial-localized catalase, which can detoxify SOD-generated hydrogen peroxide, also produced no growth benefit in the *gas-1(fc21)* mutant (Figure S3B). These results argue against decreased mitochondrial ROS toxicity underlying the rescue by hypoxia because mitochondrial ROS levels were not elevated in the complex I mutants, and over-expression of ROS-detoxifying enzymes had no benefit.

## Complex I levels are compromised in oxygen-sensitive mutants but not necessarily rescued by hypoxia or *nuo-3(G60D)*

We sought to understand what biochemical features are shared between the complex I mutants amenable to rescue by hypoxia or *nuo-3(G60D)* and whether such features underlie this rescue. First, we purified mitochondria from *nduf-7(et19)* and *gas-1(fc21)* mutants and profiled their OXPHOS complexes using blue native PAGE (BN-PAGE). We observed a dramatic loss of assembled complex I in the *nduf-7(et19)* mutant at all oxygen tensions, which was not rescued by *nuo-3(G60D)* or hypoxia (Figures 4A, 4B, and S4A). A faint new band running below the complex V dimer also appeared in *nduf-7(et19)* (Figure S4A). Native gel followed by western blot for hemagglutinin (HA)-tagged NDUFAB1/NDAB-1 revealed subcomplexes in *nduf-7(et19)* that may correspond to complex I degradation products (Figure S4B). Similarly, loss of *Ndufs4* in mice causes a fragile complex I prone to degradation.[37,38] The *gas-1(fc21)* mutant also showed a pronounced loss of assembled complex I which was exacerbated at 50% oxygen, and *nuo-3(G60D)* rescued levels of assembled complex I in this mutant (Figures 4A, 4B, and S4C). These results suggest that complex I instability may be a common trait in mutants whose growth is modified by environmental oxygen, but because *nduf-7(et19)* growth rate is rescued by hypoxia and *nuo-3(G60D)* without restoring the levels of assembled complex I, we further investigated the specific effects of *nuo-3(G60D)* on complex I levels and activity.

Concomitant with assembly defects, loss of complex I accessory subunits can lead to degradation of other subunits within the same structural module.[3] We performed quantitative proteomics using tandem mass tags (TMT) to assess how the *C. elegans* complex I mutations and the *nuo-3(G60D)* suppressor mutation affect levels of individual complex I proteins. We quantified over 7,000 proteins, including 36/42 subunits of *C. elegans* complex I. In concordance with our BN-PAGE observations (Figures 4A and 4B), multiple complex I subunits were lost in *nduf-7(et19)* and *gas-1(fc21)* at 50% oxygen, whereas subunits of ETC complexes II–V were unchanged (Figures 4C, 4D, S4D, and S4E). In particular, Q module and N module complex I subunits were depleted, consistent with structural defects in the soluble arm of complex I. Introduction of the *nuo-3(G60D)* suppressor mutation rescued the loss of Q and N module proteins in the *gas-1(fc21)* mutant at 50% oxygen, but not in the *nduf-7(et19)* mutant, in line with BN-PAGE results (Figure 4E). We validated these high throughput results with SDS-PAGE western blots against Q module subunits NDUFS3/NUO-2 and NDUFS6/NDUF-6. At 21% and 50% oxygen we observed loss of these complex I subunits in *nduf-7(et19)* and *gas-1(fc21)*, which was rescued by *nuo-3(G60D)* only in *gas-1(fc21)* (Figures 4F and 4G). Notably, the effects of hypoxia treatment on complex I mutants *nduf-7(et19)* and *gas-1(fc21)* phenocopied the *nuo-3(G60D)* mutant: NDUFS3/NUO-2 and NDUFS6/NDUF-6 levels were rescued by 1% oxygen in the *gas-1(fc21)* mutant but not in *nduf-7(et19)* (Figure 4G). The identical effects on complex I levels by hypoxia and *nuo-3(G60D)* further support a shared mechanism of action. Given that hypoxia and *nuo-3(G60D)* improve the growth and development of *nduf-7(et19)* without a restoration of complex I levels, the underlying rescue mechanism is unlikely to be a restoration of complex I stability.

Loss of complex I levels may reflect a general dysfunction in iron-sulfur (Fe-S) cluster synthesis or instability of Fe-S containing proteins, two phenomena that are sensitive to excess molecular oxygen.[39,40] To address this possibility, we measured steady-state Fe-S clusters in *C. elegans* complex I mutants. Lipoic acid is a protein modification generated by lipoic acid synthetase, which requires mitochondrially produced Fe-S clusters. Neither *gas-1(fc21)* nor *nduf-7(et19)* showed any deficit in lipoic acid levels at 1%, 21%, or 50% oxygen (Figure S4F), indicating that steady-state Fe-S levels were not compromised in these mutants. We also analyzed the levels of 50 Fe-S-containing proteins in our TMT proteomics data and observed no general decrease of these proteins in the *gas-1(fc21)* and *nduf-7(et19)* mutants, apart from complex I subunits (Figures S4G and S4H). These data argue against hypoxia rescuing complex I mutants through a general effect on Fe-S cluster synthesis or stability and support our model that hypoxia acts specifically on complex I.

## *NDUFA6/nuo-3(G60D)* and hypoxia rescue complex I forward activity in oxygen-sensitive mutants

To determine if *nuo-3(G60D)* restores forward electron flow through the ETC, we directly measured the redox state of *C. elegans* coenzyme $Q_9$ using mass spectrometry. Validating this approach, complex I mutants showed diminished $QH_2$/Q ratios, whereas the complex III (CoQ:cytochrome *c* oxidoreductase) mutant *isp-1(qm150)* showed a ratio of $QH_2$/Q that trended higher (Figures 5A and S5A). Additionally, the endogenous CoQ biosynthesis mutant *clk-1(qm30)* produced no detectable $Q_9$ or $Q_9H_2$ (Figure S5B), demonstrating the specificity of this assay. The *nuo-3(G60D)* suppressor mutation

Please cite this article in press as: Meisel et al., Hypoxia and intra-complex genetic suppressors rescue complex I mutants by a shared mechanism, Cell (2024), https://doi.org/10.1016/j.cell.2023.12.010



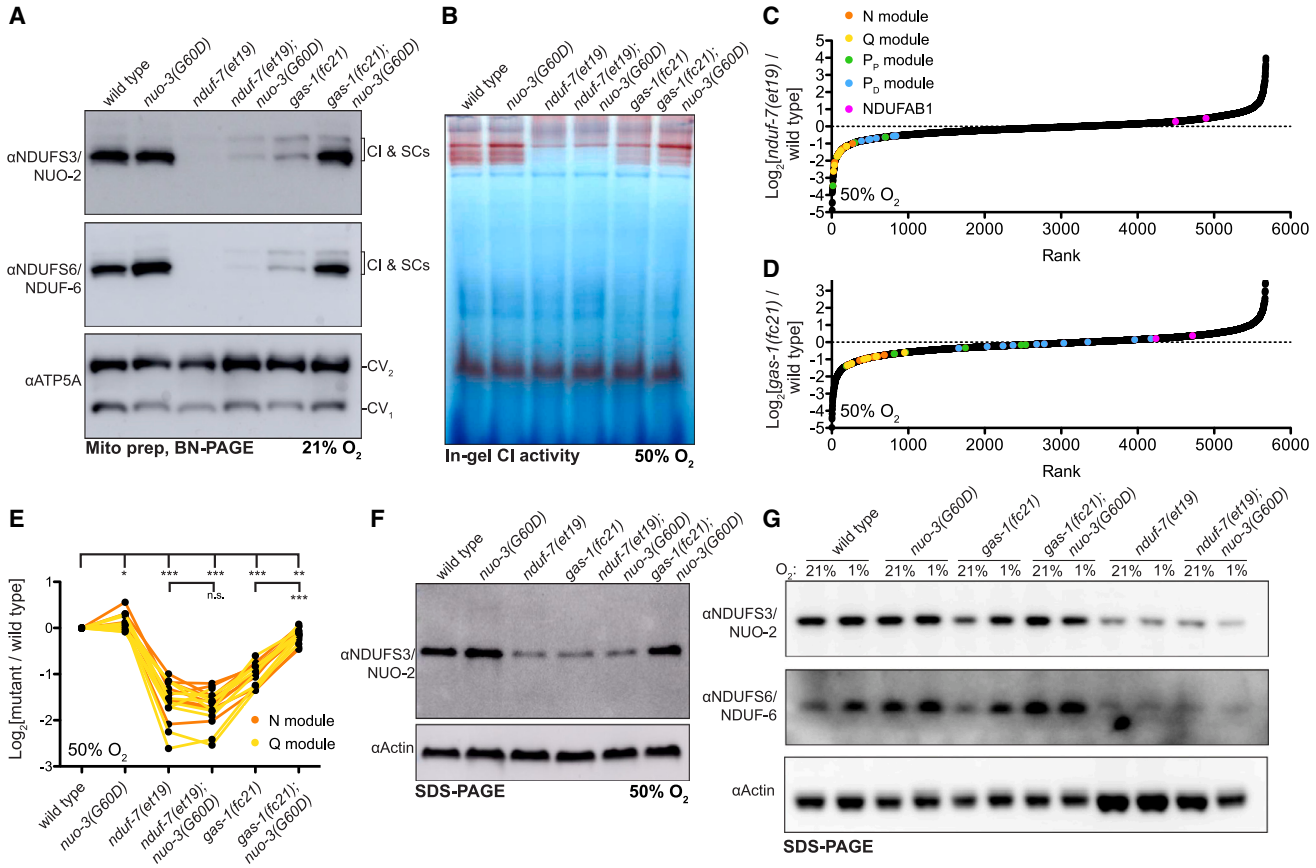


**Figure 4. Complex I levels are compromised in oxygen-sensitive mutants, but their restoration does not underlie the rescue by hypoxia or *nuo-3(G60D)***

(A) BN-PAGE of isolated mitochondria followed by western blot from animals grown continuously at 21% oxygen.

(B) BN-PAGE of isolated mitochondria followed by complex I in-gel dehydrogenase activity assay from animals exposed to 50% oxygen for 1 day.

(C and D) TMT quantitative proteomics from animals exposed to 50% oxygen for 2 days. Plotted are log 2-fold ratios of all proteins from which at least two peptides were quantified. Complex I subunits are colored according to structural module.[4].

(E) TMT quantitative proteomics from animals exposed to 50% oxygen for 2 days. Plotted are log 2-fold ratios of all complex I N module (orange) and Q module (yellow) subunits from which at least two peptides were quantified.

(F and G) SDS-PAGE followed by western blot of whole worm lysate from animals exposed to 21%, 50%, or 1% oxygen. For all panels, statistical significance was calculated using one-way ANOVA followed by Tukey's multiple comparison test. n.s., not significant, *p value < 0.05, **p value < 0.01, ***p value < 0.001.

See also Figure S4 and Table S3.

rescued CoQ redox potential in complex I mutants *nduf-7(et19)* and *gas-1(fc21)* (Figure 5A). We also measured mitochondrial membrane potential using the fluorescent dye TMRM. *nduf-7(et19)* and *gas-1(fc21)* showed diminished TMRM fluorescence, which was partially rescued by the *nuo-3(G60D)* suppressor, consistent with an increase in proton pumping by the ETC (Figure 5B). Taken together, along with the rescue of *hsp-6::gfp* induction (Figure 2G), which is a readout of mitochondrial membrane potential and protein import efficiency, these experiments demonstrate rescue of forward electron flow through the ETC by *nuo-3(G60D)*, supporting the hypothesis that complex I activity is restored by this intra-complex mutation.

Because complex I levels in *nduf-7(et19)* are not restored by *nuo-3(G60D)* or hypoxia, despite overall growth and ETC activity being rescued, we used this mutant for further biochemical studies of complex I activity. We isolated mitochondrial membranes and performed *in vitro* assays using absorbance spectrophotometry to monitor the consumption of NADH. Wild-type NADH oxidase activity was 90% inhibited by rotenone and piericidin (complex I inhibitors) and 75% inhibited by antimycin and sodium azide (which target complexes III and IV, respectively) (Figure 5C), confirming the activity was complex I and ETC dependent. We measured NADH oxidase activity from *nduf-7(et19)* mutant membranes and observed a 50% reduction in complex I activity which was partially rescued by the *nuo-3(G60D)* suppressor (Figure 5D). We confirmed through western blot of the same mitochondrial membranes that complex I levels were not changed in the *nduf-7(et19); nuo-3(G60D)* double mutant (Figure S5C), despite the increase in NADH oxidation rate. These data demonstrate that *nuo-3(G60D)* can restore mutant complex I forward activity independent of complex I

Please cite this article in press as: Meisel et al., Hypoxia and intra-complex genetic suppressors rescue complex I mutants by a shared mechanism, Cell (2024), https://doi.org/10.1016/j.cell.2023.12.010



CellPress
OPEN ACCESS

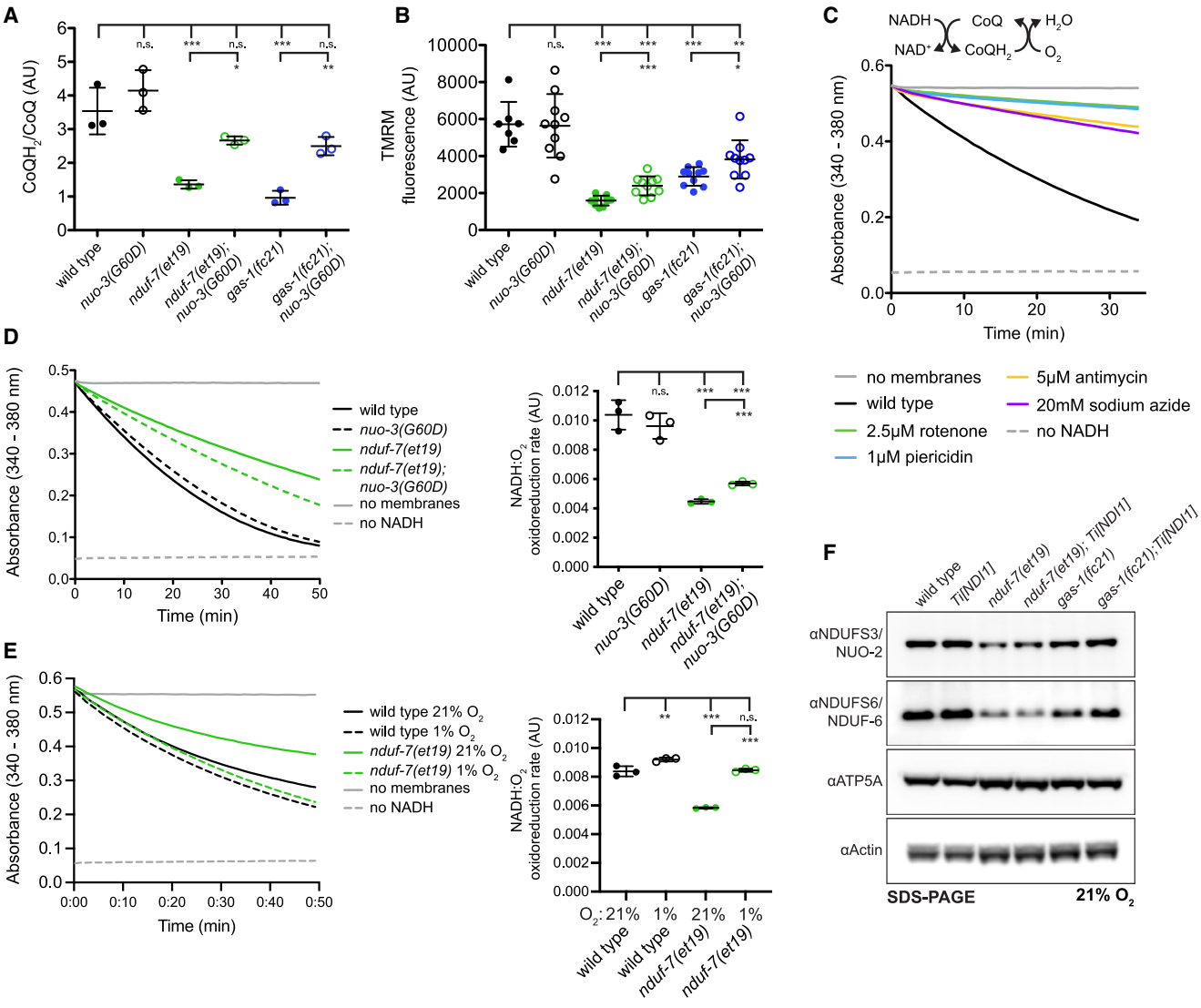


**Figure 5. *NDUFA6/nuo-3(G60D)* and hypoxia rescue complex I forward activity in oxygen-sensitive mutants**

(A) Ratio of reduced $CoQ_9H_2$ to oxidized $CoQ_9$ as determined by mass spectrometry. Samples were extracted from whole worms grown continuously at 21% oxygen.

(B) TMRM fluorescence quantified by measuring the mean fluorescence in the posterior bulb of the pharynx after 1 day at 21% oxygen. Images were taken with an exposure time of 20 ms at 63× magnification.

(C–E) Complex I-dependent oxidation of NADH by isolated mitochondrial membranes *in vitro*. NADH absorbs light at 340 nm. Plotted (at right) are rates of absorbance at 340 nm (minus 380 nm) per minute from the first 20 min of linear slopes.

(F) SDS-PAGE followed by western blot of whole worm lysate from animals exposed to 21% oxygen. *Ti[NDI1]* animals contain a single-copy integrated transgene expressing mito-targeted NDI1. For all panels, statistical significance was calculated using one-way ANOVA followed by Tukey's multiple comparison test. Error bars represent standard deviation. n.s., not significant, *p value < 0.05, **p value < 0.01, ***p value < 0.001.

See also Figure S5.

levels, explaining the rescue of downstream ETC flux and growth. We then performed the same complex I activity assay using wild-type and *nduf-7(et19)* membranes in a hypoxia cabinet. Strikingly, we observed that acute incubation at 1% oxygen was also able to increase the NADH oxidation rate from *nduf-7(et19)* mutant membranes *in vitro* (Figure 5E), showing that hypoxia, like *nuo-3(G60D)*, can directly restore the forward activity of complex I.

## Restored ETC flux is upstream of complex I protein level rescue

To untangle the effects of *nuo-3(G60D)* in the *gas-1(fc21)* mutant, where complex I levels are restored (Figures 4A and 4B), we took advantage of the yeast NDI1 bypass of complex I deficiency, which restores electron flow from NADH to CoQ. *nduf-7(et19)* and *gas-1(fc21)* mutants rescued by single-copy integrated NDI1 were tested for complex I subunit levels. Although NDI1

Please cite this article in press as: Meisel et al., Hypoxia and intra-complex genetic suppressors rescue complex I mutants by a shared mechanism, Cell (2024), https://doi.org/10.1016/j.cell.2023.12.010



rescued the slow growth of both mutants, complex I levels were partially restored only in *gas-1(fc21)* (Figures 5F and S5D). This pattern matches exactly the effects of hypoxia and *nuo-3(G60D)* and proves that restoration of ETC flux is sufficient (i.e., upstream) of complex I level rescue in the *gas-1(fc21)* mutant. Our model is that *nuo-3(G60D)* and hypoxia restore complex I forward activity, with many downstream consequences such as increased proton pumping, oxygen consumption, ATP production, and, in the case of some mutants, complex I levels.

Complex I subunit levels are decreased in the brains of *Ndufs4* knockout mice,[37,38] and we measured the effects of two hypoxia regimes that improve the disease phenotype in these animals. We observed a modest increase in the levels of NDUFS1, NDUFS6, NDUFS3, and NDUFA9 in both a "prevention" paradigm[11] where 11% oxygen treatment began at weaning (days 25–30) and a "rescue" paradigm[12] in which mice were exposed to 21% oxygen for 55 days until they developed advanced disease symptoms and then transferred to 11% oxygen (Figure S5E). Similarly, in *C. elegans*, the *NDUFS4lpd-5(mg746); nuo-3(G60D)* double mutant, which is fertile at 1% oxygen (Figure S2E) and thus can be probed by western blot, displayed complex I levels that were sensitive to increasing amounts of oxygen (Figure S5F). In concordance, the *lpd-5(mg746); nuo-3(G60D)* double mutant was sensitive to 50% oxygen (Figure S5G). Taken together, these results show that hypoxia restores complex I levels in *NDUFS4* mutants as it does in *gas-1(fc21)*.

## Complex I rescue by *NDUFA6/nuo-3(G60D)* requires LYRM domain activity

To better understand the mechanism of how *nuo-3(G60D)* leads to increased complex I forward activity in complex I mutants, we generated transgenic animals expressing *nuo-3* variants with a wild-type *nuo-3* gene at the endogenous locus. Over-expression of *nuo-3(G60D)* but not wild-type *nuo-3* suppressed *gas-1(fc21)* and *nduf-7(et19)* sensitivity to hyperoxia (Figures 6A and 6B), supporting a dominant gain-of-function mode of action for the G60D mutation (as opposed to increased wild-type function). Transgenic rescue of *gas-1(fc21)* by *nuo-3(G60D)* was not as effective as mutating the endogenous *nuo-3* locus, suggesting that competition with wild-type NUO-3 for inclusion in complex I was detrimental to growth in hyperoxia (Figure S6A). To confirm that both transgenes were functional, we generated a *nuo-3* null allele using CRISPR that we found arrested development at an early larval stage in 21% and 1% oxygen (Figure S6B). Either *nuo-3(wt)* or *nuo-3(G60D)* transgenes could rescue the lethality of the *nuo-3(null)* (Figure S6C), confirming their functionality.

Glycine 60 of NDUFA6/NUO-3 lies within the conserved LYRM domain responsible for binding the acyl carrier protein (NDUFAB1 or ACP) to complex I[41] (Figure 6C). The motif is characterized by an L-Y-R tripeptide followed by a downstream F, and mutation of these residues in the yeast *Yarrowia lipolytica* partially reduces ACP binding and complex I activity.[42] To test if altering LYRM domain activity would affect the function of NUO-3 in the context of complex I rescue, we generated *nuo-3* transgenes containing the F70A mutation. Neither *nuo-3(F70A)* nor *nuo-3(G60D F70A)* could suppress *gas-1(fc21)* sensitivity to hyperoxia, demonstrating that LYRM domain activity is required for the *nuo-3(G60D)* suppression (Figure 6D). In *C. elegans* and other nematodes, the L-Y-R sequence is replaced by the functionally adjacent A-Y-K (Figure S6D). We introduced Y38A K39A substitutions into *nuo-3* transgenes and again found the rescue of *gas-1(fc21)* by *nuo-3(G60D)* to be abolished when LYRM domain activity was compromised (Figure 6E). Importantly, *nuo-3(G60D F70A)* and *nuo-3(Y38A K39A G60D)* transgenes were both able to partially rescue the growth and fertility defects of the *nuo-3(null)* mutant, demonstrating that these protein variants were still functional (Figure 6F). Taken together, this argues against *nuo-3(G60D)* acting as a dominant negative, as weakening the LYRM domain is insufficient to rescue complex I mutants and in fact shows a requirement for LYRM domain activity (i.e., ACP binding) in the action of the *nuo-3(G60D)* suppressor.

To further explore how the G60D substitution affects the function of NUO-3, we used CRISPR-Cas9 editing followed by homologous repair with degenerate oligos to generate all possible G60 missense mutations at the chromosomal *nuo-3* locus in a single experiment. In a wild-type background, all G60 substitutions are tolerated with no discernable effects on growth (Figure S6E). To our surprise, many G60 amino acid substitutions were able to rescue the developmental arrest of NDUFS4/*lpd-5* null animals at 21% oxygen, including R, K, D, H, T, V, I, M, L, F, and W (Figures 6G and 6H). However, the sterically small amino acids with side chains of 0–1 carbons (e.g., G, A, or S) as well as proline did not rescue complex I mutants (Figures 6G and 6H). These results are in concordance with our genetic screen, which used a mutagen that favors G-to-A or C-to-T transitions and could thus only isolate G60D or G60S substitutions. Interestingly, when comparing NUO-3 sequences across nematode evolution, we found that NUO-3 amino acid 60 is conserved as either a G, S, or P (Figure S6D), suggesting selection for these small side-chain amino acids in normal complex I function. NUO-3(G60) lies near the end of the alpha helix that surrounds the NDUFAB1 acyl chain, and residues such as G and P tend to break alpha helices.[43] Outside essential features of the LYRM domain, the primary sequence of NDUFA6/NUO-3 has diverged across eukaryotic evolution, and *nuo-3(G60)* may correspond to a lysine residue in mammals or be functionally analogous to NDUFA6(G59) (Figure S6D). An intriguing possibility is that in the context of NDUFS4 loss, mutating this residue to a larger amino acid may stabilize the alpha helix and enhance binding to NDUFAB1.

## Residues surrounding the CoQ binding cavity are required for complex I rescue by *NDUFA6/nuo-3(G60D)* or hypoxia

Complex I mutants *nduf-7(et19)* and *gas-1(fc21)* are sensitive to low doses of the complex I inhibitor rotenone (0.1 μM)—a concentration that does not affect the growth of wild-type animals—likely due to additive inhibitory effects on complex I (Figure S7A). Surprisingly, *nuo-3(G60D)* as a single mutant was hypersensitive to rotenone, which was especially evident at higher doses of 0.5 and 1.0 μM (Figures 7A and S7A). Rotenone is a plant-derived inhibitor of complex I that occupies the quinone binding pocket.[25] Expression of the yeast complex I

Please cite this article in press as: Meisel et al., Hypoxia and intra-complex genetic suppressors rescue complex I mutants by a shared mechanism, Cell (2024), https://doi.org/10.1016/j.cell.2023.12.010



CellPress
OPEN ACCESS

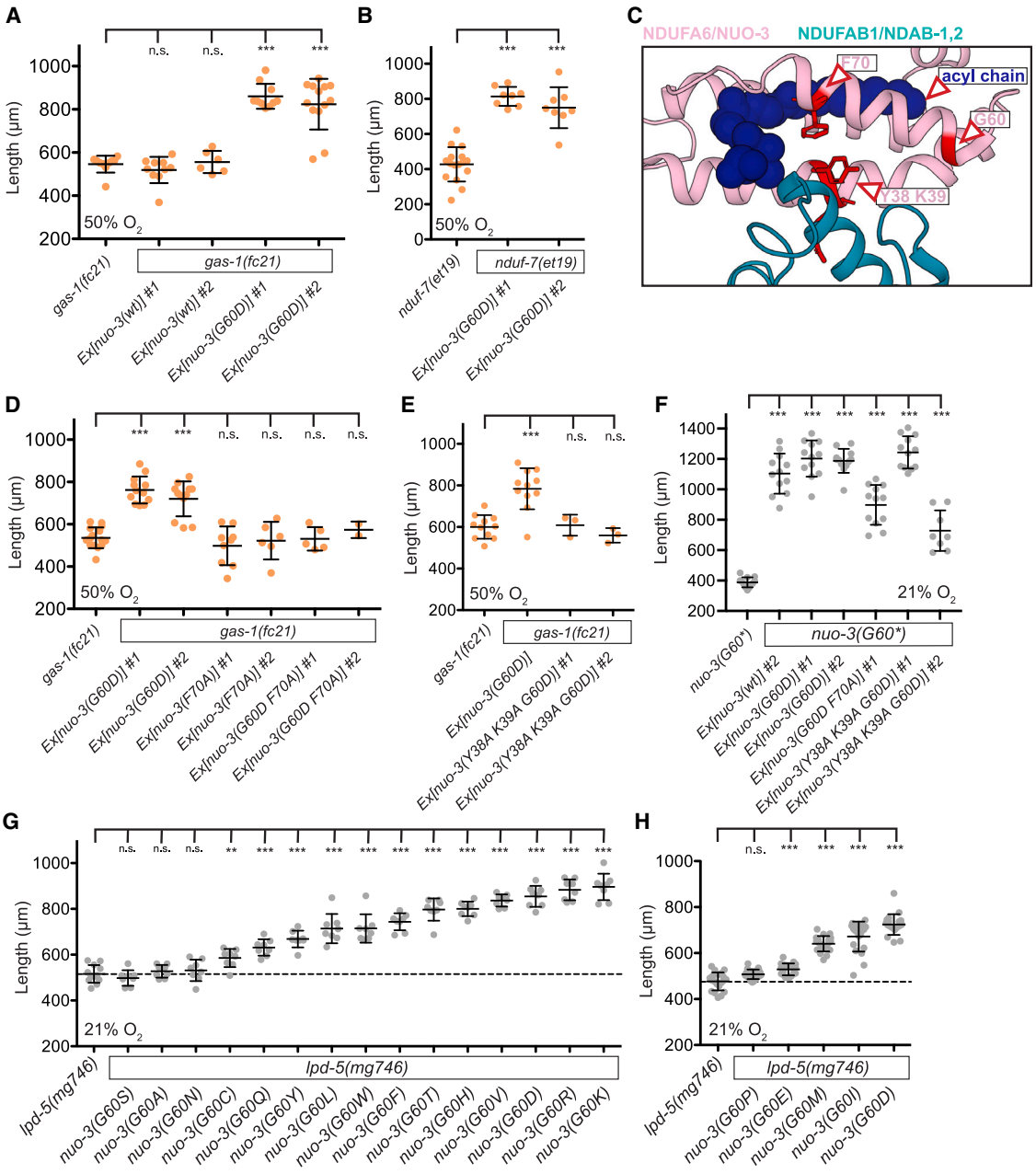


**Figure 6. Complex I rescue by *NDUFA6/nuo-3(G60D)* requires LYRM domain activity**

(A) Growth of animals for 5 days at 50% oxygen followed by 1 day at 21% oxygen.

(B) Growth of animals for 5 days at 50% oxygen followed by 3 days at 21% oxygen.

(C) Ovine complex I (PDB: 6ZKC[25]) in closed conformation. Colored red is the residue corresponding to *C. elegans nuo-3(G60D)* based on homology modeling. Colored red and represented as sticks are residues corresponding to *C. elegans* LYRM residues Y38, K39, and F70.

(D and E) Growth of animals for 6 days at 50% oxygen.

(F) Growth of animals for 5 days at 21% oxygen at 20°C.

(G and H) Growth of animals for 3 days at 21% oxygen incubated at 20°C. For all panels, statistical significance was calculated using one-way ANOVA followed by Tukey's multiple comparison test or Dunnett's multiple comparison test (G and H). Error bars represent standard deviation. n.s., not significant, *p value < 0.05, **p value < 0.01, ***p value < 0.001.

See also Figure S6.

bypass protein NDI1 rendered wild-type *C. elegans* rotenone-resistant, proving that rotenone inhibits *C. elegans* growth rate by the inhibition of complex I (Figure S7B). Sensitivity of *nuo-3(G60D)* to rotenone may imply a change in conformation near the rotenone/CoQ binding site, which is consistent with NUO-3/NUYM mutations in *Yarrowia* having long-range effects on complex I structure that disrupt the formation of loops required for CoQ redox chemistry.[44] These results revealed that the *nuo-3(G60D)* mutant harbors a liability to growth in rotenone, potentially explaining the presence of G, S, and P residues at this site in evolution and presenting an opportunity to screen for rare suppressor mutations.

To understand the downstream effectors of *nuo-3(G60D)* rescue, we performed a forward genetic screen for suppressors of *NDUFA6/nuo-3(G60D)* growth arrest on rotenone (Figure 7B). Following sequencing of the nuclear genome and mtDNA, we identified four independent alleles of *NDUFS7/nduf-7*, one allele of *NDUFS2/gas-1*, and eight alleles of *MED15/mdt-15* (Table S2). CRISPR-Cas9 generated alleles in a *nuo-3(G60D)* background suppressed the rotenone hypersensitivity phenotype, confirming the genetic identity of these suppressor mutations (Figures 7C and S7C). Based on high-resolution structures, the CoQ binding pocket within complex I is defined by mobile loops emanating from NDUFS2, NDUFS7, ND1, and ND3.[45–47] Strikingly, the mutations we isolated in complex I subunits were amino acid substitutions in three highly conserved residues surrounding the CoQ/rotenone binding cavity: NDUFS2/GAS-1(V161I), NDUFS7/NDUF-7(A119T or A119V), and NDUFS7/NDUF-7(M80I) (Figures 7D and S7D). Unlike the complex I mutants *gas-1(fc21)* and *nduf-7(et19)* used for much of the analysis above, the *nduf-7* and *gas-1* amino acid substitution mutations isolated as *nuo-3(G60D)* suppressors do not grow slowly at 21% oxygen, nor are they sensitive to 50% oxygen (Figures S7E and S7F). The multiple *mdt-15* alleles that emerged from the rotenone resistance screen may activate rotenone detoxification. *mdt-15* encodes a component of the Mediator transcriptional regulatory complex that controls drug detoxification; gain-of-function mutations in *mdt-15*, including the same P117L substitution mutation isolated in our screen, activate *C. elegans* xenobiotic detoxification pathways.[48] All mutations isolated for *NDUFA6/nuo-3(G60D)* rotenone resistance confer partial resistance to rotenone in a *NDUFA6/nuo-3* wild-type background (Figure S7B). Thus, complex I structural changes that prevent rotenone binding (in the case of the *nduf-7* and *gas-1* amino acid substitution mutations) or activation of a rotenone detoxifying response (in the case of *mdt-15*) mediate the *nuo-3(G60D)* suppression. Taken together, these results suggest that *nuo-3(G60D)* causes long-range conformational changes around the CoQ binding site that render animals hypersensitive to rotenone.

We tested whether the same suppressor mutations that rescue the hypersensitivity of *nuo-3(G60D)* to rotenone would also block the beneficial effects *nuo-3(G60D)* has on oxygen-sensitive complex I mutants. Indeed, introduction of *gas-1(V161I)* or *nduf-7(M80I)* mutation completely suppressed the rescue of *NDUFS4/lpd-5(mg746)* by *nuo-3(G60D)* (Figures 7E and 7F), identifying a downstream genetic requirement for the restoration of complex I activity. *nduf-7(A119V)* mutation partially suppressed the rescue of *lpd-5(mg746)* by *nuo-3(G60D)* (Figure 7E), consistent with its weaker rotenone resistance phenotype. *mdt-15(P117L)* had no effect on rescue of *lpd-5(mg746) by nuo-3(G60D)* (Figure 7G), consistent with its mechanism of action being complex I-independent activation of rotenone detoxification. Importantly, the *gas-1(V161I)* mutation did not affect the growth rates of the *lpd-5(mg746)* or *nuo-3(G60D)* single mutants (Figures 7F and S7G), demonstrating no synthetic sickness but rather a specific activity for this mutation in blocking rescue of complex I activity by *nuo-3(G60D)*. The overlapping genetic requirements for the beneficial and harmful effects of *nuo-3(G60D)* suggest that the same structural changes that produce rotenone sensitivity also underlie the rescue of *NDUFS4/lpd-5(mg746)*, perhaps due to increasing accessibility of rotenone and CoQ, respectively. Conversely, the *nuo-3(G60D)* suppressor mutations (i.e., *gas-1(V161I)*) may decrease the accessibility of rotenone and CoQ to the cavity, leading to their rotenone resistance and blockage of complex I rescue.

To further elucidate the effects of *gas-1(V161I)* and *nduf-7(A119V)* suppressor mutations on complex I, we isolated mitochondrial membranes from these mutants (in an otherwise wild-type background) and performed *in vitro* experiments using absorbance spectrophotometry. Western blotting revealed that complex I levels were not decreased in these mutant membranes but rather slightly increased (Figure S7H). NADH oxidase activity was also not compromised in these mutants (Figure S7I), indicating that the flow of electrons from NADH to CoQ remains unchanged. However, NADH-driven ROS production (without piericidin) was decreased in *gas-1(V161I)* and *nduf-7(A119V)* (Figure 7H), consistent with these mutations decreasing accessibility of the CoQ binding pocket, reducing the leak of electrons to molecular oxygen. By contrast, ROS production from complex I in the presence of piericidin, which blocks electron flow and is a readout of the flavin site reducing molecular oxygen, was unchanged in the mutants (Figure 7H), consistent with overall complex I levels being unaffected.

Finally, we asked if the genetic requirements for complex I rescue by *NDUFA6/nuo-3(G60D)* were also necessary for the beneficial effects of hypoxia on complex I mutants. The *NDUFS2/gas-1(V161I)* mutation significantly blunted the rescue of *NDUFS4/lpd-5(mg746)* by hypoxia in a *nuo-3(wt)* background (Figure 7I), identifying a "hypoxia-resistant" mutation that blocks hypoxia rescue of complex I dysfunction and further suggesting the rescue by hypoxia and *nuo-3(G60D)* may share a common mechanism. *nduf-7(A119V)* and *mdt-15(P117L)* had no effect on *lpd-5(mg746)* growth in hypoxia (Figure 7I), consistent with the former's weaker *nuo-3(G60D)* suppression phenotype and the latter's complex I-independent mode of action. Unlike *hif-1(ia4)* null animals, none of the *nuo-3(G60D)* suppressors were sensitive to hypoxia on their own (Figure S7J), supporting a specific effect of *gas-1(V161I)* on the *NDUFS4/lpd-5*-hypoxia interaction. These data suggest that hypoxia is beneficial to complex I mutants in a manner dependent on residues in the CoQ binding pocket, supporting a model in which hypoxia promotes forward flow through complex I (Figure 7J).

## DISCUSSION

Complex I, the main entry point of energy into the ETC, is an ancient complex whose 14 core subunits are evolutionarily

Please cite this article in press as: Meisel et al., Hypoxia and intra-complex genetic suppressors rescue complex I mutants by a shared mechanism, Cell (2024), https://doi.org/10.1016/j.cell.2023.12.010





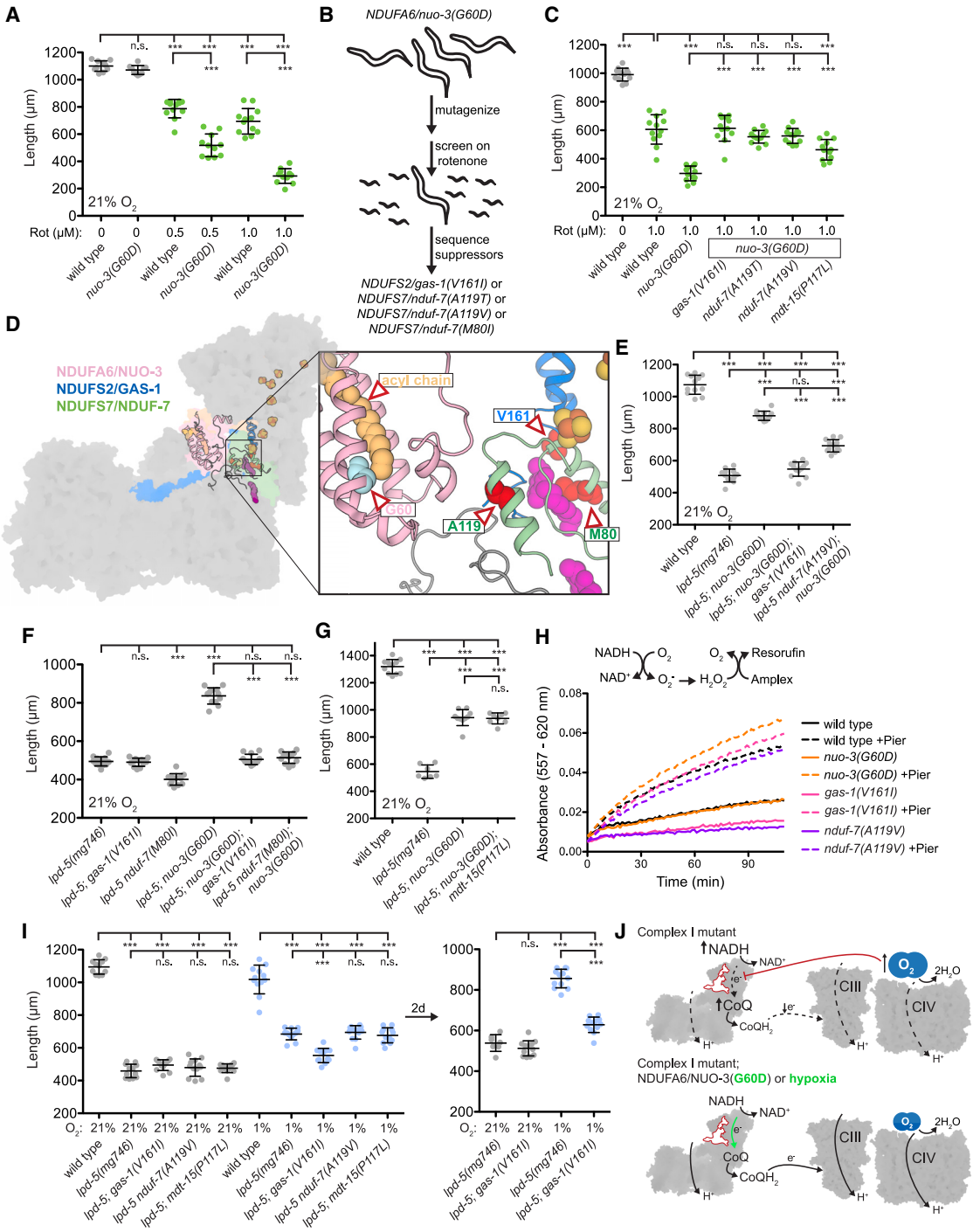


**Figure 7. Mutations surrounding the CoQ binding pocket block the ability of *NDUFA6/nuo-3(G60D)* or hypoxia to rescue complex I**

(A) Growth of animals for 3 days at 21% oxygen with 0, 0.5, or 1.0 µM rotenone.

(B) *nuo-3(G60D)* P0 animals were randomly mutagenized with EMS in the absence of rotenone. F2 progeny were transferred to rotenone-containing plates and selected for growth.

(C) Growth of animals for 2 days at 21% oxygen incubated at room temperature with 0 or 1.0 µM rotenone.

(D) Ovine complex I (PDB: 6ZKC[25]) in closed conformation. Labeled and colored red are residues corresponding to *C. elegans nuo-3(G60D)* suppressor mutations NDUFS2/GAS-1(V161I), NDUFS7/NDUF-7(A119T or A119V), and NDUFS7/NDUF-7(M80I). Decylubiquinone is colored magenta.

(E and F) Growth of animals for 3 days at 21% oxygen incubated at 20°C.

(G) Growth of animals for 4 days at 21% oxygen incubated at room temperature.

*(legend continued on next page)*

Please cite this article in press as: Meisel et al., Hypoxia and intra-complex genetic suppressors rescue complex I mutants by a shared mechanism, Cell (2024), https://doi.org/10.1016/j.cell.2023.12.010



conserved across all major domains of life.[49] In recent years, advances in structural biology have deepened our understanding of the macromolecular organization of complex I, revealing an Fe-S cluster electron transfer path in the soluble arm of complex I that ultimately reduces CoQ and induces proton pumping across the membrane arm to store energy.[45–47] But exactly how CoQ reduction transduces proton pumping across the membrane arm remains actively debated, and what role eukaryotic-specific accessory subunits may have in this mechanism is unknown. The current genetic study has revealed the existence of a dense, oxygen-sensitive network within complex I (involving accessory subunits NDUFA6 and NDUFAB1) with effects centered on the CoQ binding pocket (Figures 7D and 7J). These genetic interactions likely reflect allosteric coupling between an accessory subunit and energy conversion centers within complex I that arose through co-evolution of this complex with fluctuations of ambient oxygen that occur over evolutionary, developmental, and physiological timescales.

Our mechanistic study was initially motivated by the discovery that low oxygen can rescue phenotypes of the *Ndufs4* knockout mouse.[11] We now find that the ability of hypoxia to rescue *NDUFS4* knockout is evolutionarily conserved to *C. elegans*. We tested a total of nine *C. elegans* complex I mutants for rescue by hypoxia and found that only those mutations that partially compromise the matrix arm of complex I could be suppressed by hypoxia. Our *in vivo* results from *C. elegans* are distinct from a genome-wide CRISPR screen performed in mammalian K562 cells at differing oxygen tensions, which found nearly all complex I subunit knockouts were rescued at 1% oxygen.[50] This discordance may reflect the fact that cell culture models are more tolerant of mitochondrial dysfunction. In fact, rho0 cells altogether lacking mtDNA and the respiratory chain can be grown if supplemented with glucose, pyruvate, and uridine.[51] Given that human disease-causing mutations in complex I are widely distributed throughout the complex and give rise to heterogeneous phenotypes,[5] these results may help predict which human mutations are "oxygen-sensitive" and hence candidates for hypoxia-based therapy.

To further explore the genetics of *C. elegans* complex I mutations that are suppressed by hypoxia, we took advantage of the sensitivity of complex I mutants to 50% oxygen. The use of this moderate hyperoxia regime has physiological relevance, as brains of *Ndufs4* knockout mice experience local hyperoxia, likely due to reduced ETC activity and less associated oxygen consumption.[13] We identified a *C. elegans* intra-complex I mutation, *NDUFA6/nuo-3(G60D)*, capable of rescuing all three complex I mutants rescued by hypoxia. These mutations are distributed across the soluble matrix arm, leading us to hypothesize that *NDUFA6/nuo-3(G60D)* is generally protective to this specific class of complex I mutants. Using *in vitro* biochemical assays, we showed that *NDUFA6/nuo-3(G60D)* rescues complex I forward activity—the flow of electrons from NADH to CoQ—while not necessarily restoring complex I protein levels. These data are consistent with a model in which *nuo-3(G60D)* mutation alters complex I structure around the CoQ binding pocket to create a more active enzyme in these mutant backgrounds. This change in activity will lead to more oxygen consumption at complex IV, lowering local oxygen levels which may further stabilize the fragile matrix arm, consistent with proposed models[40] (Figure 7J). The downstream consequences on the cell include more mitochondrial ATP production, increased membrane potential, and normalized NADH/$NAD^+$ balance. These factors individually or in combination likely contribute to the growth benefit of the complex I mutants.

To discover the downstream effectors of the rescue by *NDUFA6/nuo-3(G60D)*, we took advantage of the hypersensitivity of this mutant to rotenone—a feature consistent with increased accessibility of the rotenone/CoQ binding pocket. We performed a forward genetic screen to identify *nuo-3(G60D)* suppressor mutations and identified conserved residues in NDUFS2/GAS-1 and NDUFS7/NDUF-7 surrounding the CoQ binding pocket (Figure 7D) that are necessary for the effects of *NDUFA6/nuo-3(G60D)* on rotenone sensitivity and complex I rescue. Two of these residues, NDUFS2/GAS-1(V161) and NDUFS7/NDUF-7(M80), were previously found through mutational studies in *Yarrowia* to define the CoQ binding pocket and be important for complex I activity but not complex I abundance.[52,53] Our combined genetics and biochemistry support a model in which *nuo-3(G60D)* alters complex I conformation to enhance binding of both the natural electron acceptor ubiquinone and the ubiquinone competitive inhibitor rotenone, and mutations identified in our suppressor screen such as *NDUFS2/gas-1(V161I)* revert these effects. These data are consistent with work from *Yarrowia* demonstrating NDUFA6 mutations trigger long-range conformational changes that impact the Q binding site[44] and support a model in which increased forward activity of complex I precedes the restoration of complex I stability in oxygen-sensitive mutants.

Four lines of evidence support the model that *NDUFA6/nuo-3(G60D)* is a "hypoxia-mimetic" mutation that rescues complex I deficiency by a mechanism that is similar to hypoxia: (1) the subset of complex I lesions rescued by *nuo-3(G60D)* and hypoxia are identical, (2) *nuo-3(G60D)* protects these complex I mutants against moderate hyperoxia, (3) *nuo-3(G60D)* and hypoxia have identical effects on complex I protein levels and complex I activity, and (4) the same mutation, *NDUFS2/gas-1(V161I)*, blocks the rescue by *nuo-3(G60D)* or hypoxia, jointly pointing to a shared rescue mechanism. The acute rescuing effects of

(H) NADH-driven complex I-dependent superoxide production in the presence or absence of piericidin by isolated mitochondrial membranes at 21% oxygen. Resorufin absorbs light at 557 nm.

(I) Growth of animals for 3 days (left) and 5 days (right) at 21% or 1% oxygen incubated at room temperature.

(J) Complex I mutations result in decreased flux through the ETC, leading to local hyperoxia, which can further inhibit complex I activity. Hypoxia or *NDUFA6/nuo-3(G60D)* mutation restore complex I forward activity in a manner dependent on residues surrounding the CoQ binding cavity. For all panels, statistical significance was calculated using one-way ANOVA followed by Tukey's multiple comparison test. Error bars represent standard deviation. n.s., not significant, *p value < 0.05, **p value < 0.01, ***p value < 0.001.

See also Figure S7.

hypoxia on complex I activity *in vitro*, combined with the identification of *NDUFS2/gas-1(V161I)* as a "drug-resistant" mutant for hypoxia rescue, strongly support the model that hypoxia acts like *nuo-3(G60D)* to rescue complex I activity either through triggering a structural change near the CoQ binding pocket, or alternatively by altering the local chemical environment.

The NDUFA6/NUO-3(G60D) residue lies in the conserved LYRM domain of NDUFA6, responsible for tethering the acyl carrier protein NDUFAB1/ACP to complex I.[41] We show through structure-function studies that LYRM domain activity is required for *nuo-3(G60D)* suppression activity. NDUFAB1 is one of the last accessory subunits to be incorporated into complex I and is essential for its assembly and function.[3,4,54] Additionally, NDUFAB1 can bind to other LYRM domain-containing proteins and is required for at least two more essential processes in the mitochondria: it is the scaffold upon which type II fatty acid synthesis proceeds,[55] an upstream requirement for protein lipoylation, and it is an essential component of the Fe-S cluster biosynthesis machinery.[56] *C. elegans* and mammalian mutants in Fe-S cluster biosynthesis are rescued by hypoxia,[39] and all the above NDUFAB1-dependent processes were found to be selectively essential at 21% oxygen (i.e., rescued by hypoxia) in a genome-wide CRISPR screen.[50] We therefore hypothesize that NDUFAB1 may coordinate a general response to oxygen in the mitochondria. Our mutational studies at the NUO-3(G60) site revealed that many amino acid substitutions can rescue *NDUFS4/lpd-5* loss, arguing against a strong structural role for the G60 residue (e.g., salt bridge, polar contacts) and suggesting that the local dynamics of this region near the end of the NDUFAB1 acyl chain have important consequences for complex I activity. Interestingly there is precedent for NDUFAB1 overexpression in mice increasing complex I formation and providing protection from ischemia-reperfusion injury.[57]

Most components of the mitochondrial ETC, including many complex I proteins, are conserved across major domains of life including bacteria and archaea.[49] Hence, these ETC components evolved in the last universal common ancestor (LUCA) prior to the great oxygenation event almost 3 billion years ago[58] by using terminal electron acceptors other than oxygen. Many ecological niches today continue to be anaerobic, where microbes couple their ETC to terminal electron acceptors such as nitrate, sulfate, or ferric iron. Tantalizingly, the NDUFS7/NDUF-7(M80I) mutation is present in many bacterial species that grow in anaerobic environments, and the NDUFS7/NDUF-7(A119V) mutation is present in yeast (Figure S7D), showing that our mutants reflect existing natural variations that have been selected for in microbial evolution. Even among diverse eukaryotes that have evolved during the past billion years, hypoxia is often encountered in their normal life cycles,[59] for example, in deep water, crowded ecosystems, or poorly vascularized mammalian tumors. Thus, hypoxia treatment of mitochondrial disease marshals for medicine ancient and highly evolved adaptations of the ETC to natural oxygen tension changes.

### Limitations of the study

This work demonstrates that some, but not all, *C. elegans* complex I mutants are rescued by hypoxia and sensitive to high oxygen. For these mutants, the underlying mechanism of hypoxia rescue is a restoration of complex I activity. In some but not all cases, a restoration of ETC flux leads to an increase in complex I protein levels, likely due to decreased molecular oxygen. In agreement, we observed a small increase in complex I levels in the brains of *Ndufs4* mice exposed to hypoxia. Future work in mammals is required to determine if the rescue of complex I mutants by hypoxia is also due to an increase in complex I activity. Our hypoxia-mimetic and hypoxia-resistant mutations point to the CoQ binding pocket as a site of action of hypoxia—either through inducing allosteric structural changes or by altering quinone chemistry. Structural studies of *C. elegans* complex I in our mutant backgrounds, or mammalian complex I in hypoxia, may help to reveal chemical or conformation changes that restore the flow of electrons from NADH to ubiquinone.

## STAR★METHODS

Detailed methods are provided in the online version of this paper and include the following:

- KEY RESOURCES TABLE
- RESOURCE AVAILABILITY
  - Lead contact
  - Materials availability
  - Data and code availability
- EXPERIMENTAL MODELS AND STUDY PARTICIPANT DETAILS
  - *C. elegans* strain maintenance
  - Mouse strains, husbandry, and hypoxia exposure
- METHOD DETAILS
  - *C. elegans* strain generation
  - Growth and fluorescent reporter assays
  - Genetic screens and sequence analysis
  - Mitochondrial biochemistry
  - Mass spectrometry
- QUANTIFICATION AND STATISTICAL ANALYSIS

### SUPPLEMENTAL INFORMATION

Supplemental information can be found online at https://doi.org/10.1016/j.cell.2023.12.010.

### ACKNOWLEDGMENTS

We thank Peter Breen, Connie Chan, Sarah Chang, Thomas Hercher, Sharon Kim, Andrew Markhard, and Jason McCoy for technical assistance. We thank Zenon Grabarek and all members of the Mootha and Ruvkun labs for helpful discussions. This work was supported in part by the National Institutes of Health (K99GM140217 to J.D.M., F32GM133047 to O.S.S., R01AG016636 to G.R., and R01NS124679 to V.K.M.). J.D.M. was supported by The Jane Coffin Childs Memorial Fund for Medical Research. M.M. was supported by the Deutsche Forschungsgemeinschaft (431313887). V.K.M. is an Investigator of the Howard Hughes Medical Institute.

### AUTHOR CONTRIBUTIONS

Conceptualization, J.D.M., G.R., and V.K.M.; methodology, J.D.M., M.M., O.S.S., and A.A.J.; investigation, J.D.M., M.M., O.S.S., P.P.W., S.M.W., and A.A.J.; writing – original draft, J.D.M.; writing – review & editing, J.D.M., M.M., O.S.S., P.P.W., S.M.W., A.A.J., G.R., and V.K.M.; supervision, G.R. and V.K.M.; funding acquisition, J.D.M., G.R., and V.K.M.

## DECLARATION OF INTERESTS

V.K.M. is listed as an inventor on patents filed by MGH on therapeutic uses of hypoxia. V.K.M. is a paid advisor to 5am Ventures. O.S.S. was a paid consultant for Proteinaceous, Inc. V.K.M. is on the Advisory Board at *Cell*.

Received: February 20, 2023
Revised: September 9, 2023
Accepted: December 5, 2023
Published: January 11, 2024

## REFERENCES

1. Hirst, J. (2013). Mitochondrial complex I. Annu. Rev. Biochem. *82*, 551–575.
2. Sazanov, L.A. (2015). A giant molecular proton pump: structure and mechanism of respiratory complex I. Nat. Rev. Mol. Cell Biol. *16*, 375–388.
3. Stroud, D.A., Surgenor, E.E., Formosa, L.E., Reljic, B., Frazier, A.E., Dibley, M.G., Osellame, L.D., Stait, T., Beilharz, T.H., Thorburn, D.R., et al. (2016). Accessory subunits are integral for assembly and function of human mitochondrial complex I. Nature *538*, 123–126.
4. Guerrero-Castillo, S., Baertling, F., Kownatzki, D., Wessels, H.J., Arnold, S., Brandt, U., and Nijtmans, L. (2017). The assembly pathway of mitochondrial respiratory chain complex I. Cell Metab. *25*, 128–139.
5. Fiedorczuk, K., and Sazanov, L.A. (2018). Mammalian mitochondrial complex I structure and disease-causing mutations. Trends Cell Biol. *28*, 835–867.
6. Russell, O.M., Gorman, G.S., Lightowlers, R.N., and Turnbull, D.M. (2020). Mitochondrial diseases: hope for the future. Cell *181*, 168–188.
7. Frazier, A.E., Thorburn, D.R., and Compton, A.G. (2019). Mitochondrial energy generation disorders: genes, mechanisms, and clues to pathology. J. Biol. Chem. *294*, 5386–5395.
8. Schapira, A.H.V., Cooper, J.M., Dexter, D., Jenner, P., Clark, J.B., and Marsden, C.D. (1989). Mitochondrial complex I deficiency in Parkinson's disease. Lancet *1*, 1269.
9. Gopal, R.K., Calvo, S.E., Shih, A.R., Chaves, F.L., McGuone, D., Mick, E., Pierce, K.A., Li, Y., Garofalo, A., Van Allen, E.M.V., et al. (2018). Early loss of mitochondrial complex I and rewiring of glutathione metabolism in renal oncocytoma. Proc. Natl. Acad. Sci. USA *115*, E6283–E6290.
10. Gopal, R.K., Kübler, K., Calvo, S.E., Polak, P., Livitz, D., Rosebrock, D., Sadow, P.M., Campbell, B., Donovan, S.E., Amin, S., et al. (2017). Widespread chromosomal losses and mitochondrial DNA alterations as genetic drivers in Hürthle cell carcinoma. Cancer Cell *34*, 242–255.e5.
11. Jain, I.H., Zazzeron, L., Goli, R., Alexa, K., Schatzman-Bone, S., Dhillon, H., Goldberger, O., Peng, J., Shalem, O., Sanjana, N.E., et al. (2016). Hypoxia as a therapy for mitochondrial disease. Science *352*, 54–61.
12. Ferrari, M., Jain, I.H., Goldberger, O., Rezoagli, E., Thoonen, R., Cheng, K.H., Sosnovik, D.E., Scherrer-Crosbie, M., Mootha, V.K., and Zapol, W.M. (2017). Hypoxia treatment reverses neurodegenerative disease in a mouse model of Leigh syndrome. Proc. Natl. Acad. Sci. USA *114*, E4241–E4250.
13. Jain, I.H., Zazzeron, L., Goldberger, O., Marutani, E., Wojtkiewicz, G.R., Ast, T., Wang, H., Schleifer, G., Stepanova, A., Brepoels, K., et al. (2019). Leigh syndrome mouse model can be rescued by interventions that normalize brain hyperoxia, but not HIF activation. Cell Metab. *30*, 824–832.e3.
14. Falk, M.J., Rosenjack, J.R., Polyak, E., Suthammarak, W., Chen, Z., Morgan, P.G., and Sedensky, M.M. (2009). Subcomplex Iλ specifically controls integrated mitochondrial functions in Caenorhabditis elegans. PLoS One *4*, e6607.
15. Kayser, E.B., Morgan, P.G., Hoppel, C.L., and Sedensky, M.M. (2001). Mitochondrial expression and function of GAS-1 in Caenorhabditis elegans. J. Biol. Chem. *276*, 20551–20558.
16. Kayser, E.B., Morgan, P.G., and Sedensky, M.M. (1999). GAS-1: a mitochondrial protein controls sensitivity to volatile anesthetics in the nematode Caenorhabditis elegans. Anesthesiology *90*, 545–554.
17. Yang, W., and Hekimi, S. (2010). Two modes of mitochondrial dysfunction lead independently to lifespan extension in Caenorhabditis elegans. Aging Cell *9*, 433–447.
18. Rauthan, M., Ranji, P., Abukar, R., and Pilon, M. (2015). A mutation in Caenorhabditis elegans NDUF-7 activates the mitochondrial stress response and prolongs lifespan via ROS and CED-4. G3 (Bethesda) *5*, 1639–1648.
19. Félix, M.A., and Duveau, F. (2012). Population dynamics and habitat sharing of natural populations of Caenorhabditis elegans and C. briggsae. BMC Biol. *10*, 59.
20. Gray, J.M., Karow, D.S., Lu, H., Chang, A.J., Chang, J.S., Ellis, R.E., Marletta, M.A., and Bargmann, C.I. (2004). Oxygen sensation and social feeding mediated by a C. elegans guanylate cyclase homologue. Nature *430*, 317–322.
21. Van Voorhies, W.A.V., and Ward, S. (2000). Broad oxygen tolerance in the nematode Caenorhabditis elegans. J. Exp. Biol. *203*, 2467–2478.
22. Jafari, G., Wasko, B.M., Tonge, A., Schurman, N., Dong, C., Li, Z., Peters, R., Kayser, E.B., Pitt, J.N., Morgan, P.G., et al. (2015). Tether mutations that restore function and suppress pleiotropic phenotypes of the C. elegans isp-1(qm150) Rieske iron-sulfur protein. Proc. Natl. Acad. Sci. USA *112*, E6148–E6157.
23. Hartman, P.S., Ishii, N., Kayser, E.B., Morgan, P.G., and Sedensky, M.M. (2001). Mitochondrial mutations differentially affect aging, mutability and anesthetic sensitivity in Caenorhabditis elegans. Mech. Ageing Dev. *122*, 1187–1201.
24. Ishii, N., Takahashi, K., Tomita, S., Keino, T., Honda, S., Yoshino, K., and Suzuki, K. (1990). A methyl viologen-sensitive mutant of the nematode Caenorhabditis elegans. Mutat. Res. DNAging *237*, 165–171.
25. Kampjut, D., and Sazanov, L.A. (2020). The coupling mechanism of mammalian respiratory complex I. Science *370*.
26. Shpilka, T., Du, Y., Yang, Q., Melber, A., Uma Naresh, N.U., Lavelle, J., Kim, S., Liu, P., Weidberg, H., Li, R., et al. (2021). UPRmt scales mitochondrial network expansion with protein synthesis via mitochondrial import in Caenorhabditis elegans. Nat. Commun. *12*, 479.
27. Haynes, C.M., Yang, Y., Blais, S.P., Neubert, T.A., and Ron, D. (2010). The matrix peptide exporter HAF-1 signals a mitochondrial UPR by activating the transcription factor ZC376.7 in C. elegans. Mol. Cell *37*, 529–540.
28. Marres, C.A.M., de Vries, S., and Grivell, L.A. (1991). Isolation and inactivation of the nuclear gene encoding the rotenone-insensitive internal NADH: ubiquinone oxidoreductase of mitochondria from Saccharomyces cerevisiae. Eur. J. Biochem. *195*, 857–862.
29. Cossard, R., Esposito, M., Sellem, C.H., Pitayu, L., Vasnier, C., Delahodde, A., and Dassa, E.P. (2015). Caenorhabditis elegans expressing the Saccharomyces cerevisiae NADH alternative dehydrogenase Ndi1p, as a tool to identify new genes involved in complex I related diseases. Front. Genet. *6*, 206.
30. DeCorby, A., Gášková, D., Sayles, L.C., and Lemire, B.D. (2007). Expression of Ndi1p, an alternative NADH:ubiquinone oxidoreductase, increases mitochondrial membrane potential in a C. elegans model of mitochondrial disease. Biochim. Biophys. Acta *1767*, 1157–1163.
31. McElroy, G.S., Reczek, C.R., Reyfman, P.A., Mithal, D.S., Horbinski, C.M., and Chandel, N.S. (2020). $NAD^+$ regeneration rescues lifespan, but not ataxia, in a mouse model of brain mitochondrial complex I dysfunction. Cell Metab. *32*, 301–308.e6.
32. Ohh, M., Park, C.W., Ivan, M., Hoffman, M.A., Kim, T.Y., Huang, L.E., Pavletich, N., Chau, V., and Kaelin, W.G. (2000). Ubiquitination of hypoxia-inducible factor requires direct binding to the β-domain of the von Hippel–Lindau protein. Nat. Cell Biol. *2*, 423–427.
33. Govindan, J.A., Jayamani, E., and Ruvkun, G. (2019). ROS-based lethality of Caenorhabditis elegans mitochondrial electron transport mutants

grown on Escherichia coli siderophore iron release mutants. Proc. Natl. Acad. Sci. USA *116*, 21651–21658.

34. Chen, S., Luo, S., Zhang, Z., and Ma, D.K. (2019). VHL-1 inactivation and mitochondrial antioxidants rescue C. elegans dopaminergic neurodegeneration. Protein Cell *10*, 610–614.
35. Dancy, B.M., Brockway, N., Ramadasan-Nair, R., Yang, Y., Sedensky, M.M., and Morgan, P.G. (2016). Glutathione S-transferase mediates an ageing response to mitochondrial dysfunction. Mech. Ageing Dev. *153*, 14–21.
36. Dalleau, S., Baradat, M., Guéraud, F., and Huc, L. (2013). Cell death and diseases related to oxidative stress: 4-hydroxynonenal (HNE) in the balance. Cell Death Differ. *20*, 1615–1630.
37. Kruse, S.E., Watt, W.C., Marcinek, D.J., Kapur, R.P., Schenkman, K.A., and Palmiter, R.D. (2008). Mice with mitochondrial complex I deficiency develop a fatal encephalomyopathy. Cell Metab. *7*, 312–320.
38. Adjobo-Hermans, M.J.W., Haas, R. de, Willems, P.H.G.M., Wojtala, A., Vries, S.E.van E., Wagenaars, J.A., Brand, M. van den, Rodenburg, R.J., Smeitink, J.A.M., Nijtmans, L.G., et al. (2020). NDUFS4 deletion triggers loss of NDUFA12 in Ndufs4-/- mice and Leigh syndrome patients: a stabilizing role for NDUFAF2. Biochim. Biophys. Acta Bioenerg. *1861*, 148213.
39. Ast, T., Meisel, J.D., Patra, S., Wang, H., Grange, R.M.H., Kim, S.H., Calvo, S.E., Orefice, L.L., Nagashima, F., Ichinose, F., et al. (2019). Hypoxia rescues frataxin loss by restoring iron sulfur cluster biogenesis. Cell *177*, 1507–1521.e16.
40. Baik, A.H., Haribowo, A.G., Chen, X., Queliconi, B.B., Barrios, A.M., Garg, A., Maishan, M., Campos, A.R., Matthay, M.A., and Jain, I.H. (2023). Oxygen toxicity causes cyclic damage by destabilizing specific Fe-S cluster-containing protein complexes. Mol. Cell *83*, 942–960.e9.
41. Angerer, H. (2015). Eukaryotic LYR proteins interact with mitochondrial protein complexes. Biology *4*, 133–150.
42. Angerer, H., Radermacher, M., Mańkowska, M., Steger, M., Zwicker, K., Heide, H., Wittig, I., Brandt, U., and Zickermann, V. (2014). The LYR protein subunit NB4M/NDUFA6 of mitochondrial complex I anchors an acyl carrier protein and is essential for catalytic activity. Proc. Natl. Acad. Sci. USA *111*, 5207–5212.
43. Chou, P.Y., and Fasman, G.D. (1979). Advances in enzymology and related areas of molecular biology. In Prediction of the Secondary Structure of Proteins from their Amino Acid Sequence, A. Meister, ed. (John Wiley & Sons, Inc.).
44. Galemou Yoga, E., Parey, K., Djurabekova, A., Haapanen, O., Siegmund, K., Zwicker, K., Sharma, V., Zickermann, V., and Angerer, H. (2020). Essential role of accessory subunit LYRM6 in the mechanism of mitochondrial complex I. Nat. Commun. *11*, 6008.
45. Zhu, J., Vinothkumar, K.R., and Hirst, J. (2016). Structure of mammalian respiratory complex I. Nature *536*, 354–358.
46. Fiedorczuk, K., Letts, J.A., Degliesposti, G., Kaszuba, K., Skehel, M., and Sazanov, L.A. (2016). Atomic structure of the entire mammalian mitochondrial complex I. Nature *538*, 406–410.
47. Zickermann, V., Wirth, C., Nasiri, H., Siegmund, K., Schwalbe, H., Hunte, C., and Brandt, U. (2015). Structural biology. Mechanistic insight from the crystal structure of mitochondrial complex I. Science *347*, 44–49.
48. Mao, K., Ji, F., Breen, P., Sewell, A., Han, M., Sadreyev, R., and Ruvkun, G. (2019). Mitochondrial dysfunction in C. elegans activates mitochondrial relocalization and nuclear hormone receptor-dependent detoxification genes. Cell Metab. *29*, 1182–1191.e4.
49. Gabaldón, T., Rainey, D., and Huynen, M.A. (2005). Tracing the evolution of a large protein complex in the eukaryotes, NADH:ubiquinone oxidoreductase (complex I). J. Mol. Biol. *348*, 857–870.
50. Jain, I.H., Calvo, S.E., Markhard, A.L., Skinner, O.S., To, T.-L., Ast, T., and Mootha, V.K. (2019). Genetic screen for cell fitness in high or low oxygen highlights mitochondrial and lipid metabolism. Cell *181*, 716–727.e11.
51. King, M.P., and Attardi, G. (1989). Human cells lacking mtDNA: repopulation with exogenous mitochondria by complementation. Science *246*, 500–503.
52. Tocilescu, M.A., Fendel, U., Zwicker, K., Kerscher, S., and Brandt, U. (2007). Exploring the ubiquinone binding cavity of respiratory complex I. J. Biol. Chem. *282*, 29514–29520.
53. Angerer, H., Nasiri, H.R., Niedergesäß, V., Kerscher, S., Schwalbe, H., and Brandt, U. (2012). Tracing the tail of ubiquinone in mitochondrial complex I. Biochim. Biophys. Acta *1817*, 1776–1784.
54. Sackmann, U., Zensen, R., Röhlen, D., Jahnke, U., and Weiss, H. (1991). The acyl-carrier protein in Neurospora crassa mitochondria is a subunit of NADH:ubiquinone reductase (complex I). Eur. J. Biochem. *200*, 463–469.
55. Mikolajczyk, S., and Brody, S. (1990). De novo fatty acid synthesis mediated by acyl-carrier protein in Neurospora crassa mitochondria. Eur. J. Biochem. *187*, 431–437.
56. Van Vranken, J.G.V., Jeong, M.Y., Wei, P., Chen, Y.C., Gygi, S.P., Winge, D.R., and Rutter, J. (2016). The mitochondrial acyl carrier protein (ACP) coordinates mitochondrial fatty acid synthesis with iron sulfur cluster biogenesis. eLife *5*, 174.
57. Hou, T., Zhang, R., Jian, C., Ding, W., Wang, Y., Ling, S., Ma, Q., Hu, X., Cheng, H., and Wang, X. (2019). NDUFAB1 confers cardio-protection by enhancing mitochondrial bioenergetics through coordination of respiratory complex and supercomplex assembly. Cell Res. *29*, 754–766.
58. Canfield, D.E. (2005). THE EARLY HISTORY OF ATMOSPHERIC OXYGEN: homage to Robert M. Garrels. Annu. Rev. Earth Planet. Sci. *33*, 1–36.
59. Müller, M., Mentel, M., Hellemond, J.J. van, Henze, K., Woehle, C., Gould, S.B., Yu, R.Y., Giezen, M. van der, Tielens, A.G.M., and Martin, W.F. (2012). Biochemistry and evolution of anaerobic energy metabolism in eukaryotes. Microbiol. Mol. Biol. Rev. *76*, 444–495.
60. Brenner, S. (1974). The genetics of Caenorhabditis elegans. Genetics *77*, 71–94.
61. Quintana, A., Kruse, S.E., Kapur, R.P., Sanz, E., and Palmiter, R.D. (2010). Complex I deficiency due to loss of Ndufs4 in the brain results in progressive encephalopathy resembling Leigh syndrome. Proc. Natl. Acad. Sci. USA *107*, 10996–11001.
62. Ghanta, K.S., and Mello, C.C. (2020). Melting dsDNA donor molecules greatly improves precision genome editing in Caenorhabditis elegans. Genetics *216*, 643–650.
63. Arribere, J.A., Bell, R.T., Fu, B.X.H., Artiles, K.L., Hartman, P.S., and Fire, A.Z. (2014). Efficient marker-free recovery of custom genetic modifications with CRISPR/Cas9 in Caenorhabditis elegans. Genetics *198*, 837–846.
64. Frøkjær-Jensen, C., Davis, M.W., Sarov, M., Taylor, J., Flibotte, S., LaBella, M., Pozniakovsky, A., Moerman, D.G., and Jorgensen, E.M. (2014). Random and targeted transgene insertion in Caenorhabditis elegans using a modified Mos1 transposon. Nat. Methods *11*, 529–534.
65. Lehrbach, N.J., Ji, F., and Sadreyev, R. (2017). Next-generation sequencing for identification of EMS-induced mutations in Caenorhabditis elegans. Curr. Protoc. Mol. Biol. *117*, 7.29.1–7.29.12.
66. Yin, Z., Burger, N., Kula-Alwar, D., Aksentijević, D., Bridges, H.R., Prag, H.A., Grba, D.N., Viscomi, C., James, A.M., Mottahedin, A., et al. (2021). Structural basis for a complex I mutation that blocks pathological ROS production. Nat. Commun. *12*, 707.
67. Andreini, C., Banci, L., and Rosato, A. (2016). Exploiting bacterial operons to illuminate human iron-sulfur proteins. J. Proteome Res. *15*, 1308–1322.

Please cite this article in press as: Meisel et al., Hypoxia and intra-complex genetic suppressors rescue complex I mutants by a shared mechanism, Cell (2024), https://doi.org/10.1016/j.cell.2023.12.010



## STAR★METHODS

### KEY RESOURCES TABLE

| REAGENT or RESOURCE | SOURCE | IDENTIFIER |
|---|---|---|
| **Antibodies** | | |
| Anti-NDUFS3 (mouse) | Abcam | Abcam Cat# ab14711; RRID:AB_301429 |
| Anti-NDUFS6 (rabbit) | Abcam | ab195807 |
| Anti-NDUFS1 (rabbit) | Abcam | ab185733 |
| Anti-NDUFA9 (mouse) | Abcam | Abcam Cat# ab14713; RRID:AB_301431 |
| Anti-ATP5A (mouse) | Abcam | Abcam Cat# ab14748; RRID:AB_301447 |
| Anti-actin (rabbit) | Abcam | Abcam Cat# ab179467; RRID:AB_2737344 |
| Anti-HA (rabbit) | Abcam | Abcam Cat# ab236632; RRID:AB_2864361 |
| Anti alpha-tubulin (11H10) (rabbit) | Cell signaling | Cell Signaling Technology Cat# 2125S; RRID:AB_2619646 |
| Anti-Lipoic acid (rabbit) | Sigma (Calbiochem) | Millipore Cat# 437695; RRID:AB_212120 |
| Anti-HNE (rabbit) | Sigma (Calbiochem) | Millipore Cat# 393206; RRID:AB_211975 |
| **Bacterial and virus strains** | | |
| *E. coli* OP50 | CGC | RRID:WB-STRAIN: WBStrain00041969 |
| **Chemicals, peptides, and recombinant proteins** | | |
| Rotenone | Cayman chemical | 13995 |
| MitoSOX Red | ThermoFisher | M36008 |
| Ethyl methanesulfonate | Sigma | M0880 |
| Subtilisin A protease | Sigma | P5380 |
| Digitonin | Sigma | 300410 |
| Cytochrome c | Sigma | C7752 |
| Alamethicin | Sigma | A4665 |
| Iodonitrotetrazolium chloride | Sigma | I8377 |
| NADH | Sigma | N8129 |
| HRP | Sigma | 516531 |
| SOD | Sigma | S5395 |
| Amplex Red | ThermoFisher | A12222 |
| TMRM | ThermoFisher | T668 |
| Antimycin A | Sigma | A8674 |
| Sodium azide | Sigma | 71289 |
| **Experimental models: Organisms/strains** | | |
| *C. elegans* strain CB5602: *vhl-1(ok161)* X | CGC | CB5602 |
| *C. elegans* strain CW152: *gas-1(fc21)* X | CGC | CW152 |
| *C. elegans* strain MQ130: *clk-1(qm30)* III | CGC | MQ130 |
| *C. elegans* strain MQ1333: *nuo-6(qm200)* I | CGC | MQ1333 |
| *C. elegans* strain MQ887: *isp-1(qm150)* IV | CGC | MQ887 |
| *C. elegans* strain N2: wild type | CGC | N2 |
| *C. elegans* strain SJ4100: *zcIs13[hsp-6::GFP]* V | CGC | SJ4100 |

(*Continued on next page*)

Please cite this article in press as: Meisel et al., Hypoxia and intra-complex genetic suppressors rescue complex I mutants by a shared mechanism, Cell (2024), https://doi.org/10.1016/j.cell.2023.12.010





*Continued*

| REAGENT or RESOURCE | SOURCE | IDENTIFIER |
|---|---|---|
| *C. elegans* strain TK22: *mev-1(kn1)* III | CGC | TK22 |
| *C. elegans* strain ZG31: *hif-1(ia4)* V | CGC | ZG31 |
| *C. elegans* strain FX16526: *nduf-7(tm1436)/hT2* I | Mitani | FX16526 |
| *C. elegans* strain FX18578: *nuo-5(tm2751)/nT1* V | Mitani | FX18578 |
| *C. elegans* strain FX19115: *nuo-2(tm5258)/hT2* I | Mitani | FX19115 |
| *C. elegans* strain GR3406: *lpd-5(mg746[354bp DEL])/hT2* I | This study | GR3406 |
| *C. elegans* strain GR3407: *nduf-9(mg747[578bp DEL])/qC1* III | This study | GR3407 |
| *C. elegans* strain GR3409: *lpd-5(mg746[354bp DEL])/hT2; vhl-1(ok161)* | This study | GR3409 |
| *C. elegans* strain GR3410: *lpd-5(mg746[354bp DEL])/hT2; hif-1(ia4)* | This study | GR3410 |
| *C. elegans* strain GR3411: *mgEx865[Prpl-28::NDI1 + ofm-1::gfp]* | This study | GR3411 |
| *C. elegans* strain GR3412: *lpd-5(mg746[354bp DEL])/hT2; mgEx865[Prpl-28::NDI1 + ofm-1::gfp]* | This study | GR3412 |
| *C. elegans* strain GR3413: *nduf-7(et19); zcIs13[hsp-6::GFP]* | This study | GR3413 |
| *C. elegans* strain GR3414: *zcIs13[hsp-6::GFP]; gas-1(fc21)* | This study | GR3414 |
| *C. elegans* strain GR3415: *nuo-6(qm200); zcIs13[hsp-6::GFP]* | This study | GR3415 |
| *C. elegans* strain GR3416: *lpd-5(mg746[354bp DEL])/hT2; zcIs13 [hsp-6::GFP]* | This study | GR3416 |
| *C. elegans* strain GR3417: *nuo-2(tm5258)/hT2; zcIs13[hsp-6::GFP]* | This study | GR3417 |
| *C. elegans* strain GR3418: *nduf-7(et19); vhl-1(ok161)* | This study | GR3418 |
| *C. elegans* strain GR3419: *nduf-7(et19); hif-1(ia4)* | This study | GR3419 |
| *C. elegans* strain GR3420: *nduf-7(et19); mgEx865[Prpl-28::NDI1 + ofm-1::gfp]* | This study | GR3420 |
| *C. elegans* strain GR3421: *gas-1(fc21); mgEx865[Prpl-28::NDI1 + ofm-1::gfp]* | This study | GR3421 |
| *C. elegans* strain GR3422: *nduf-9(mg747[578bp DEL])/qC1; mgEx865[Prpl-28::NDI1 + ofm-1::gfp]* | This study | GR3422 |
| *C. elegans* strain GR3423: *nuo-6(qm200); mgEx865[Prpl-28::NDI1 + ofm-1::gfp]* | This study | GR3423 |
| *C. elegans* strain GR3408: *nduf-7(et19)* I | This study, derived from QC134 (CGC) | GR3408 |
| *C. elegans* strain GR3425: *nuo-3(mg748[G60D]); zcIs13[hsp-6::GFP]* | This study | GR3425 |
| *C. elegans* strain GR3426: *nduf-7(et19); nuo-3(mg748[G60D]); zcIs13 [hsp-6::GFP]* | This study | GR3426 |
| *C. elegans* strain GR3427: *nuo-3(mg748[G60D]); zcIs13[hsp-6::GFP]; gas-1(fc21)* | This study | GR3427 |
| *C. elegans* strain GR3428: *nduf-7(et19); nuo-3(mg748[G60D])* | This study | GR3428 |
| *C. elegans* strain GR3429: *nuo-3(mg748[G60D]); gas-1(fc21)* | This study | GR3429 |
| *C. elegans* strain GR3430: *lpd-5(mg746[354bp DEL])/hT2; nuo-3(mg748[G60D])* | This study | GR3430 |
| *C. elegans* strain GR3431: *ndua-5(mg749[R126Q])* IV | This study | GR3431 |
| *C. elegans* strain GR3432: *ndua-5(mg749[R126Q]); gas-1(fc21)* | This study | GR3432 |
| *C. elegans* strain GR3433: *lpd-5(mg746[354bp DEL])/hT2; ndua-5(mg749[R126Q])* | This study | GR3433 |
| *C. elegans* strain GR3434: *nduf-7(et19); ndua-5(mg749[R126Q])* | This study | GR3434 |
| *C. elegans* strain GR3435: *nduf-9(mg747[578bp DEL])/qC1; nuo-3(mg748[G60D])* | This study | GR3435 |
| *C. elegans* strain GR3436: *nuo-6(qm200); nuo-3(mg748[G60D])* | This study | GR3436 |
| *C. elegans* strain GR3437: *isp-1(qm150) nuo-3(mg748[G60D])* | This study | GR3437 |
| *C. elegans* strain GR3438: *mev-1(kn1); nuo-3(mg748[G60D])* | This study | GR3438 |
| *C. elegans* strain GR3439: *clk-1(qm30); nuo-3(mg748[G60D])* | This study | GR3439 |
| *C. elegans* strain GR3440: *lpd-5(mg746[354bp DEL]); nuo-3(mg748[G60D])* | This study | GR3440 |
| *C. elegans* strain GR3424: *nuo-3(mg748[G60D])* IV | This study | GR3424 |

(*Continued on next page*)

*Continued*

| REAGENT or RESOURCE | SOURCE | IDENTIFIER |
|---|---|---|
| *C. elegans* strain GR3441: *unc-119(ed3); mgTi62[Prpl-28::ndab-1 cDNA::HA + unc-119(+)]* | This study | GR3441 |
| *C. elegans* strain GR3442: *nduf-7(et19); unc-119(ed3); mgTi62[Prpl-28::ndab-1 cDNA::HA + unc-119(+)]* | This study | GR3442 |
| *C. elegans* strain GR3443: *gas-1(fc21); mgEx866[Prpl-28::nuo-3 cDNA + ofm-1::gfp]* | This study | GR3443 |
| *C. elegans* strain GR3444: *gas-1(fc21); mgEx867[Prpl-28::nuo-3 cDNA + ofm-1::gfp]* | This study | GR3444 |
| *C. elegans* strain GR3445: *gas-1(fc21); mgEx868[Prpl-28::nuo-3(G60D) cDNA + ofm-1::gfp]* | This study | GR3445 |
| *C. elegans* strain GR3446: *gas-1(fc21); mgEx869[Prpl-28::nuo-3(G60D) cDNA + ofm-1::gfp]* | This study | GR3446 |
| *C. elegans* strain GR3447: *nduf-7(et19); mgEx870[Prpl-28::nuo-3(G60D) cDNA + ofm-1::gfp]* | This study | GR3447 |
| *C. elegans* strain GR3448: *nduf-7(et19); mgEx871[Prpl-28::nuo-3(G60D) cDNA + ofm-1::gfp]* | This study | GR3448 |
| *C. elegans* strain GR3449: *gas-1(fc21); mgEx872[Prpl-28::nuo-3(F70A) cDNA + ofm-1::gfp]* | This study | GR3449 |
| *C. elegans* strain GR3450: *gas-1(fc21); mgEx873[Prpl-28::nuo-3(F70A) cDNA + ofm-1::gfp]* | This study | GR3450 |
| *C. elegans* strain GR3451: *gas-1(fc21); mgEx874[Prpl-28::nuo-3(G60D F70A) cDNA + ofm-1::gfp]* | This study | GR3451 |
| *C. elegans* strain GR3452: *gas-1(fc21); mgEx875[Prpl-28::nuo-3(G60D F70A) cDNA + ofm-1::gfp]* | This study | GR3452 |
| *C. elegans* strain GR3453: *lpd-5(mg746[354bp DEL])/hT2; nuo-3(mg750[G60R])* | This study | GR3453 |
| *C. elegans* strain GR3454: *lpd-5(mg746[354bp DEL])/hT2; nuo-3(mg751[G60L])* | This study | GR3454 |
| *C. elegans* strain GR3455: *lpd-5(mg746[354bp DEL])/hT2; nuo-3(mg752[G60K])* | This study | GR3455 |
| *C. elegans* strain GR3456: *lpd-5(mg746[354bp DEL])/hT2; nuo-3(mg753[G60H])* | This study | GR3456 |
| *C. elegans* strain GR3457: *lpd-5(mg746[354bp DEL])/hT2; nuo-3(mg754[G60F])* | This study | GR3457 |
| *C. elegans* strain GR3458: *lpd-5(mg746[354bp DEL])/hT2; nuo-3(mg755[G60V])* | This study | GR3458 |
| *C. elegans* strain GR3459: *lpd-5(mg746[354bp DEL])/hT2; nuo-3(mg756[G60T])* | This study | GR3459 |
| *C. elegans* strain GR3460: *lpd-5(mg746[354bp DEL])/hT2; nuo-3(mg757[G60W])* | This study | GR3460 |
| *C. elegans* strain GR3461: *lpd-5(mg746[354bp DEL])/hT2; nuo-3(mg758[G60N])* | This study | GR3461 |
| *C. elegans* strain GR3462: *lpd-5(mg746[354bp DEL])/hT2; nuo-3(mg759[G60Q])* | This study | GR3462 |
| *C. elegans* strain GR3463: *lpd-5(mg746[354bp DEL])/hT2; nuo-3(mg760[G60S])* | This study | GR3463 |
| *C. elegans* strain GR3464: *lpd-5(mg746[354bp DEL])/hT2; nuo-3(mg761[G60C])* | This study | GR3464 |
| *C. elegans* strain GR3465: *lpd-5(mg746[354bp DEL])/hT2; nuo-3(mg762[G60A])* | This study | GR3465 |
| *C. elegans* strain GR3466: *lpd-5(mg746[354bp DEL])/hT2; nuo-3(mg763[G60Y])* | This study | GR3466 |
| *C. elegans* strain GR3467: *lpd-5(mg746)/hT2; nuo-3(mg764[G60E])* | This study | GR3467 |
| *C. elegans* strain GR3468: *lpd-5(mg746)/hT2; nuo-3(mg765[G60P])* | This study | GR3468 |

(*Continued on next page*)

Please cite this article in press as: Meisel et al., Hypoxia and intra-complex genetic suppressors rescue complex I mutants by a shared mechanism, Cell (2024), https://doi.org/10.1016/j.cell.2023.12.010





*Continued*

| REAGENT or RESOURCE | SOURCE | IDENTIFIER |
|---|---|---|
| *C. elegans* strain GR3469: *lpd-5(mg746)/hT2; nuo-3(mg766[G60I])* | This study | GR3469 |
| *C. elegans* strain GR3470: *lpd-5(mg746)/hT2; nuo-3(mg767[G60M])* | This study | GR3470 |
| *C. elegans* strain GR3471: *gas-1(fc21); mgEx876[Prpl-28::nuo-3(Y38A K39A G60D) cDNA + ofm-1::gfp]* | This study | GR3471 |
| *C. elegans* strain GR3472: *gas-1(fc21); mgEx877[Prpl-28::nuo-3(Y38A K39A G60D) cDNA + ofm-1::gfp]* | This study | GR3472 |
| *C. elegans* strain GR2251: *mdt-15(mg640[P117L]) III* | Ruvkun Lab, Mao et al.[48] | GR2251 |
| *C. elegans* strain GR3473: *nuo-3(mg748[G60D]); gas-1(mg768[V161I])* | This study | GR3473 |
| *C. elegans* strain GR3474: *nduf-7(mg769[A119T]); nuo-3(mg748[G60D])* | This study | GR3474 |
| *C. elegans* strain GR3475: *nduf-7(mg770[A119V]); nuo-3(mg748[G60D])* | This study | GR3475 |
| *C. elegans* strain GR3476: *mdt-15(mg640[P117L]); nuo-3(mg748[G60D])* | This study | GR3476 |
| *C. elegans* strain GR3477: *nduf-7(mg771[M80I]); nuo-3(mg748[G60D])* | This study | GR3477 |
| *C. elegans* strain GR3478: *lpd-5(mg746[354bp DEL])/hT2; gas-1(mg772[V161I])* | This study | GR3478 |
| *C. elegans* strain GR3479: *lpd-5(mg746[354bp DEL]) nduf-7(mg773[M80I])/hT2[nduf-7(mg774[M80I])]* | This study | GR3479 |
| *C. elegans* strain GR3480: *lpd-5(mg746[354bp DEL])/hT2; nuo-3(mg748[G60D]); gas-1(mg772[V161I])* | This study | GR3480 |
| *C. elegans* strain GR3481: *lpd-5(mg746[354bp DEL]) nduf-7(mg773[M80I])/hT2[nduf-7(mg774[M80I])]; nuo-3(mg748[G60D])* | This study | GR3481 |
| *C. elegans* strain GR3482: *lpd-5(mg746[354bp DEL]) nduf-7(mg775[A119V])/hT2; nuo-3(mg748[G60D])* | This study | GR3482 |
| *C. elegans* strain GR3483: *lpd-5(mg746[354bp DEL])/hT2; mdt-15(mg640[P117L])/hT2; nuo-3(mg748[G60D])* | This study | GR3483 |
| *C. elegans* strain GR3484: *lpd-5(mg746[354bp DEL]) nduf-7(mg775[A119V])/hT2* | This study | GR3484 |
| *C. elegans* strain GR3485: *lpd-5(mg746[354bp DEL])/hT2; mdt-15(mg640[P117L])/hT2* | This study | GR3485 |
| *C. elegans* strain GR3486: *gas-1(mg776[V161I])* X | This study | GR3486 |
| *C. elegans* strain GR3487: *nduf-7(mg777[A119T])* I | This study | GR3487 |
| *C. elegans* strain GR3488: *nduf-7(mg778[A119V])* I | This study | GR3488 |
| *C. elegans* strain GR3540: *gas-1(fc21); wuIs156[sod-2(genomic) + rol-6(su1006)]* | This study | GR3540 |
| *C. elegans* strain GR3541: *nduf-7(et19); wuIs156[sod-2(genomic) + rol-6(su1006)]* | This study | GR3541 |
| *C. elegans* strain GR3542: *gas-1(fc21); wuIs156[sod-2(genomic) + rol-6(su1006)]; mgEx892[Prpl-28::MTS::ctl-2 + ofm-1::gfp]* | This study | GR3542 |
| *C. elegans* strain GR3543: *gas-1(fc21); wuIs156[sod-2(genomic) + rol-6(su1006)]; mgEx893[Prpl-28::MTS::ctl-2 + ofm-1::gfp]* | This study | GR3543 |
| *C. elegans* strain CL2166: *dvIs19[gst-4::gfp] III* | CGC | CL2166 |
| *C. elegans* strain GR3544: *nduf-7(et19); dvIs19[gst-4::gfp]* | This study | GR3544 |
| *C. elegans* strain GR3545: *dvIs19[gst-4::gfp]; gas-1(fc21)* | This study | GR3545 |
| *C. elegans* strain GR3546: *nuo-3(mg787[G60STOP])/tmC9[F36H1.2 (tmIs1221)] IV +12.5* | This study | GR3546 |
| *C. elegans* strain GR3547: *unc-119(ed3); mgTi69[Prpl-28::NDI + unc-119(+)]* | This study | GR3547 |
| *C. elegans* strain GR3548: *nduf-7(et19); unc-119(ed3); mgTi69[Prpl-28::NDI1 + unc-119(+)]* | This study | GR3548 |
| *C. elegans* strain GR3549: *unc-119(ed3); gas-1(fc21); mgTi69[Prpl-28::NDI1 + unc-119(+)]* | This study | GR3549 |
| *C. elegans* strain GR3550: *nuo-3(mg787[G60STOP])/tmC9; mgEx894[Prpl-28::nuo-3 cDNA + ofm-1::gfp]* | This study | GR3550 |

(*Continued on next page*)

**Continued**

| REAGENT or RESOURCE | SOURCE | IDENTIFIER |
|---|---|---|
| *C. elegans* strain GR3551: *nuo-3(mg787[G60STOP])/tmC9; mgEx895[Prpl-28::nuo-3 cDNA + ofm-1::gfp]* | This study | GR3551 |
| *C. elegans* strain GR3552: *nuo-3(mg787[G60STOP])/tmC9; mgEx896[Prpl-28::nuo-3(G60D) cDNA + ofm-1::gfp]* | This study | GR3552 |
| *C. elegans* strain GR3553: *nuo-3(mg787[G60STOP])/tmC9; mgEx897[Prpl-28::nuo-3(G60D) cDNA + ofm-1::gfp]* | This study | GR3553 |
| *C. elegans* strain GR3554: *nuo-3(mg787[G60STOP])/tmC9; mgEx898[Prpl-28::nuo-3(G60D F70A) cDNA + ofm-1::gfp]* | This study | GR3554 |
| *C. elegans* strain GR3555: *nuo-3(mg787[G60STOP])/tmC9; mgEx876[Prpl-28::nuo-3(Y38A K39A G60D) cDNA + ofm-1::gfp]* | This study | GR3555 |
| *C. elegans* strain GR3556: *nuo-3(mg787[G60STOP])/tmC9; mgEx877[Prpl-28::nuo-3(Y38A K39A G60D) cDNA + ofm-1::gfp]* | This study | GR3556 |
| Mouse strain *Ndufs4*: B6.129S4-*Ndufs4*$^{tm1.1Rpa}$/J | Palmiter laboratory | RRID:IMSR_JAX:027058 |
| **Oligonucleotides** | | |
| *nuo-3(G60)* CRISPR Guide: GGACTTCATGATATGCCGCT | This study | N/A |
| *nuo-3(G60D)* CRISPR Repair Ultramer: TGGTGGGATTTCGGACTT CATGATATGCCGCTCGACGTGTTCCGTGCTGTCATCAAGAAG | This study | N/A |
| *nuo-3(G60?)* CRISPR Repair Ultramer: TGGTGGGATTTCGG ACTTCATGATATGCCGCTCnnnGTGTTCCGTGCTGTCATCAAGAAG | This study | N/A |
| nuo-3(G60STOP) CRISPR Repair Ultramer: TGGTGGGATTTCGGAC TTCATGATATGCCGCTCTGAGTGTTCCGTGCTGTCATCAAGAAG | This study | N/A |
| *ndua-5(R126)* CRISPR Guide: attacagGCCGAATATGAAC | This study | N/A |
| *ndua-5(R126Q)* CRISPR Repair Ultramer: ttaaatgctcaataattacagGC CGAATATGAACTaGAAACTACTCAGGCAATTGTTGATTCAAAA GCATGGGAGCCTCTCGT | This study | N/A |
| *nduf-7(A119)* CRISPR Guide: TCATATATGCGGCGAAGTGC | This study | N/A |
| *nduf-7(A119T)* CRISPR Repair Ultramer: TCTGGCATTTGATCATAT ATtCttCtcaaTGtAGGTGCCATTTTGTTGGTTACTGTACCG | This study | N/A |
| *nduf-7(A119V)* CRISPR Repair Ultramer: TCTGGCATTTGATCATA TATtCttCtcaaTaCAGGTGCCATTTTGTTGGTTACTGTACCG | This study | N/A |
| *gas-1(V161)* CRISPR Guide: AGCCTGCTCATTGCACATCA | This study | N/A |
| *gas-1(V161I)* CRISPR Repair Ultramer: GCCAAAGACCAAGCCTGC TCATTGCACATCATactGAtGTAATCGAGACGATCGAAGTAT | This study | N/A |
| *nduf-7(M80)* CRISPR Guide: TACCGATCCATATCATATCT | This study | N/A |
| *nduf-7(M80I)* CRISPR Repair Ultramer: GGCTCTGAAAACGACTCC GTACCGATCCATgTCgTAcCgaGGtGCgGCaAAaTGtATCATTTC GACAGCACAACATGCGAGACCGAA | This study | N/A |
| **Recombinant DNA** | | |
| Plasmid: pJDM34 [*Prpl-28::NDI1::tbb-2 3'UTR*] (Minimos) | This study | N/A |
| Plasmid: pJDM65 [*Prpl-28::nuo-3 cDNA::tbb-2 3'UTR*] (Minimos) | This study | N/A |
| Plasmid: pJDM66 [*Prpl-28::nuo-3(G60D) cDNA::tbb-2 3'UTR*] (Minimos) | This study | N/A |
| Plasmid: pJDM67 [*Prpl-28::nuo-3(F70A) cDNA::tbb-2 3'UTR*] (Minimos) | This study | N/A |
| Plasmid: pJDM68 [*Prpl-28::nuo-3(G60D F70A) cDNA::tbb-2 3'UTR*] (Minimos) | This study | N/A |
| Plasmid: pJDM76 [*Prpl-28::nuo-3(Y38A K39A G60D) cDNA::tbb-2 3'UTR*] (Minimos) | This study | N/A |
| Plasmid: pJDM86 [*Prpl-28::ndab-1 cDNA::HA::tbb-2 3'UTR*] (Minimos) | This study | N/A |
| Plasmid: pJDM117 [Prpl-28::NDI1-MTS::ctl-2::tbb-2 3'UTR] (Minimos) | This study | N/A |

Please cite this article in press as: Meisel et al., Hypoxia and intra-complex genetic suppressors rescue complex I mutants by a shared mechanism, Cell (2024), https://doi.org/10.1016/j.cell.2023.12.010





## RESOURCE AVAILABILITY

### Lead contact

Further information and requests for resources and reagents should be directed to and will be fulfilled by the lead contact, Vamsi K. Mootha (vamsi_mootha@hms.harvard.edu).

### Materials availability

*C. elegans* strains and plasmids generated in this study are available upon request from the lead contact.

### Data and code availability

- Proteomics datasets are available in Table S3. All data reported in this paper will be shared by the lead contact upon request.
- This paper does not report original code.
- Any additional information required to reanalyze the data reported in this paper is available from the lead contact upon request.

## EXPERIMENTAL MODELS AND STUDY PARTICIPANT DETAILS

### *C. elegans* strain maintenance

*C. elegans* were propagated on NGM plates seeded with *E. coli* strain OP50.[60] A complete list of strains used in this study can be found in the key resources table. Some strains were provided by the CGC, which is funded by NIH Office of Research Infrastructure Programs (P40 OD010440). Some strains were provided by the Mitani Lab through the National Bio-Resource Project of the MEXT, Japan. In concordance with *C. elegans* nomenclature and with approval from wormbase.org, C33A12.1 (ortholog of *NDUFA5*) has been renamed *ndua-5*, Y56A3A.19 (ortholog of *NDUFAB1*) has been renamed *ndab-1*, and F37C12.3 (ortholog of *NDUFAB1*) has been renamed *ndab-2*.

### Mouse strains, husbandry, and hypoxia exposure

*Ndufs4* knockout (KO) mice were generously provided by the Palmiter laboratory (University of Washington). Pups were genotyped and weaned at 25-30 d of age. All cages were provided with food and water *ad libitum* and supporting Napa gel was provided as needed. Mice were maintained in a standard 12h light-dark cycle at a temperature between 20-25°C and humidity between 30% and 70%. *Ndufs4* KO and wild-type (WT) controls were either housed in standard oxygen conditions (21% $O_2$) until day 55 when *Ndufs4* KO present advanced disease symptoms[61] ("normoxia"), in hypoxia chambers (11% O2) starting at weaning until day 55 which prevents the disease[11] ("hypoxia prevention"), or in hypoxia chambers (11% O2) starting at day 55 for 1 month which reverses the disease[12] ("hypoxia rescue"). Male and female mice were used as no sex-specific differences in disease progression have been reported or found in our experience working with these mice. For hypoxia treatments, mice were housed at ambient sea-level pressure in plexiglass chambers, and 11% $O_2$ levels were maintained OxyCycler A84XOV Multi-Chamber Dynamic Oxygen Controller (BioSpherix Ltd., Parish, NY) using nitrogen gas (Airgas). The $CO_2$ concentration in each chamber, as well as the temperature and humidity, were monitored continuously. Mice were exposed to gas treatment continuously for 24 hours per day, 7 days a week. The chambers were briefly opened three times per week to monitor health status, provide food and water, and change the cages. Mice were euthanized at the end of the experiment by harvesting vital organs under deep isoflurane anesthesia. The Massachusetts General Hospital Institutional Animal Care and Use Committee approved all animal work in this manuscript.

## METHOD DETAILS

### *C. elegans* strain generation

To generate mutants with CRISPR/Cas9, 30 pmol *S. pyogenes* Cas9 (IDT) was injected into *C. elegans* gonads along with 90 pmol tracrRNA (IDT), 95 pmol crRNA (IDT), ssODN repair template (when applicable), and 40 ng/μl PRF4::*rol-6(su1006)* plasmid was used as a marker of successful injections.[62] Alternatively, plasmids were injected encoding the Cas9 protein and guide RNA as described.[63] All guide RNAs and repair templates can be found in the key resources table. Using CRISPR/Cas9, we generated a NDUFS4/LPD-5 null allele, *mg746*, that carries a 354 bp deletion resulting in a 103 amino acid deletion plus frameshift, which can be propagated as a balanced heterozygote. We also generated a NDUFA9/NDUF-9 null allele, *mg747*, using CRISPR that carries a 578 bp deletion resulting in a 112 amino acid deletion plus frameshift, which can be propagated as a balanced heterozygote.

To generate transgenic animals carrying extra-chromosomal arrays, a mix consisting of 50 ng/μl plasmid DNA of interest and 50 ng/μl plasmid DNA containing *ofm-1::gfp* was injected into *C. elegans* P0 gonads. F1 progeny displaying the co-injection marker were singled to new plates and screened for lines in which the array was inherited by the F2 generation; at least three independent lines were generated for each construct. To generate animals carrying single-copy integrated transgenes, a plasmid mix consisting of 50 ng/μl *Mos1* transposase, 2 ng/μl *myo-2::mCherry*, 2 ng/μl *myo-3::mCherry*, and 12 ng/μl *miniMos* transgene was injected into *unc-119(ed3)* mutant *C. elegans* as described.[64] All plasmids can be found in the key resources table.

## Growth and fluorescent reporter assays

To measure *C. elegans* growth and development crowded plates of gravid animals were washed into tubes in M9 buffer [3 g $KH_2PO_4$, 6 g $Na_2HPO_4$, 5 g NaCl, 1 ml 1 M $MgSO_4$, $H_2O$ to 1 liter] and incubated with 20% bleach and 10% 5M KOH for 5 minutes while vortexing. The resulting embryos were washed 3x in M9 buffer and allowed to hatch overnight while rocking in M9. The following day arrested L1 animals were dropped onto *E. coli* OP50 plates and incubated at 20°C. For assays in hyperoxia (50% or 100% oxygen) plates were sealed in a modular chamber (Stemcell Technologies #27310) and flushed for 3 minutes with either a 50:50 mixture of oxygen and nitrogen, or with pure oxygen gas. For assays in hypoxia (1% oxygen), animals were incubated in a Hypoxic *in vitro* cabinet (Coy Laboratory Products, Inc) at room temperature. To expose developing animals to the complex I inhibitor rotenone (Cayman chemical #13995) a stock solution of 1 mM rotenone was made in DMSO, diluted in water to the appropriate concentration, and then added to NGM plates that had been pre-seeded with *E. coli*. The plates were dried in a sterile hood after which arrested larvae were added; the final concentration of DMSO in the plates was less than 0.1%. To measure animal length, images were acquired using a ZEISS Axio Zoom V16 microscope with ZEN PRO software and the midline of individual animals was quantified in FIJI software.

To measure *hsp-6::gfp* or *gst-4::gfp* fluorescence, L4 animals were mounted on agar pads, immobilized in sodium azide, and imaged at 70x magnification using a ZEISS Axio Zoom V16 microscope with ZEN PRO software. Fluorescent images were quantified by calculating the mean fluorescence along the midline of the intestine using FIJI software. For TMRM and MitoSOX assays, stock solutions of 50 mM TMRM (ThermoFisher T668) or 5 mM MitoSOX Red (ThermoFisher M36008) were prepared in DMSO. A dilution was made in M9 Buffer and added to NGM plates pre-seeded with *E. coli* for a final concentration of 200 nM TMRM or 20 μM MitoSOX and dried in the dark. L4 animals were added to TMRM or MitoSOX containing plates and incubated in the dark for 24 hours at 21% or 50% oxygen. Animals were then picked to new plates and allowed to destain for 1 hour before being mounted on agar pads and immobilized in sodium azide (for MitoSOX) or 10 mg/ml levamisole (for TMRM). Images were acquired at 63x magnification for 200 ms (TMRM) or 1 second (MitoSOX) using a ZEISS Axio Imager Z1 microscope equipped with a Zeiss AxioCam HRc digital camera. Fluorescent images were quantified by calculating the mean fluorescence in the posterior bulb of the pharynx using FIJI software.

## Genetic screens and sequence analysis

To screen for genetic suppressors of *nduf-7(et19)*, *gas-1(fc21)*, or *nuo-3(G60D)*, thousands of L4 animals were exposed to 47 mM EMS (ethyl methanesulfonate) (Sigma M0880) for four hours while rocking. Animals were then washed twice with M9 buffer and allowed to recover on standard NGM plates. F1 animals were bleach prepped as described above to generate a synchronized L1 stage population of mutagenized F2 animals, which were then dropped onto standard NGM plates at 50% oxygen (for the *nduf-7(et19)* and *gas-1(fc21)* suppressor screens) or NGM plates at 21% oxygen containing 1 μM rotenone (for the *nuo-3(G60D)* suppressor screen). Plates were checked daily and F2 individuals capable of growing to adulthood were transferred onto new plates. Fertile isolates were retested using F3 or F4 progeny to confirm their phenotype and then genomic DNA for whole genome sequencing was isolated using Gentra Puregene Tissue Kit (Qiagen 158667).

To identify candidate suppressor mutations in screen isolates we sheared genomic DNA using a Covaris S2 sonicator and prepared libraries using the NEBNext DNA library prep kit for Illumina as described.[65] Libraries with unique barcodes were quantified using the Qubit dsDNA HS Assay Kit (Life Technologies Q32851) and pooled in sets of 24 and sequenced using Illumina HiSeq. Raw FASTQ files were analyzed on the Galaxy platform (usegalaxy.org) with the following workflow: TrimGalore! to trim reads, Map with BWA to align reads to the *C. elegans* reference genome (including the mtDNA), MiModD to call variants, and SnpEff to identify mutations that may affect protein function. Lists of protein-altering mutations from each suppressor strain were then compared to identify genes with multiple mutant alleles. These candidate genes were then verified using targeted CRISPR/Cas9-based editing.

## Mitochondrial biochemistry

To isolate *C. elegans* mitochondria for downstream applications, at least four crowded 10 cm plates of mixed-stage animals were washed into M9 buffer and spun gently for 1 minute at 200g. Supernatant was removed, replaced with 10 ml fresh M9, and animals were rotated for 30-60 minutes to wash off contaminating *E. coli*. Animals were then washed twice with fresh M9, supernatant was removed, and the worm pellet placed on ice. If the mitochondria were to be used for Blue Native PAGE, 25 μl of 10 mg/ml subtilisin A protease (Sigma P5380) was added for 10 minutes. If mitochondria were to be used for SDS PAGE Western Blot or membrane isolation, no protease was added. Worms were resuspended in sucrose buffer [5 ml 1M Sucrose, 2.5 ml 0.1M Tris/MOPS pH 7.4, 0.25 ml 0.1M EGTA/Tris pH 7.4, 17.25 ml ddH2O, 1 protease inhibitor tablet], spun gently for 1 minute, supernatant removed, and resuspended in 1 ml sucrose buffer. Samples were transferred to a Dounce homogenizer fitted with the "tight" B pestle, and 40-50 strokes performed on ice. Samples were spun at 4°C for 5 minutes at 2000g, supernatants containing mitochondria transferred to new tubes, and spun again at 4°C for 10 minutes at 13,000g. Supernatant was removed, mitochondrial pellets were resuspended in sucrose buffer with pipetting, and protein concentration was measured using Bradford assay (Sigma B6916).

For assessment of ETC complexes and supercomplexes with Blue Native PAGE, 40 μl samples were prepared containing 25 μg mitochondria, 1% digitonin (Sigma 300410), NativePAGE Sample Buffer, and incubated on ice for 15 minutes. Samples were then spun at 4°C for 30 minutes at 20,000g, and supernatants were transferred to new tubes. To each sample G-250 was added to a final concentration of 0.1%, and then loaded into a 1mm thick 3-12% Native PAGE 10-well gel along with Native protein ladder (Thermo LC0725). The gel was run at 150V for 20 minutes in dark cathode buffer at 4°C, and then run at 250V for 90 minutes in light cathode buffer. If the gel was to be stained for ETC complexes, it was transferred to 40% methanol/10% acetic acid fixation solution and

Please cite this article in press as: Meisel et al., Hypoxia and intra-complex genetic suppressors rescue complex I mutants by a shared mechanism, Cell (2024), https://doi.org/10.1016/j.cell.2023.12.010



microwaved for 45 seconds at power level 10. The gel was then incubated on a rocker for 30 minutes and room temperature, rinsed with Milli-Q water, and stained with Imperial Protein Stain for 2 hours. The gel was de-stained with UltraPure water and imaged with a GE Amersham Imager. If the gel was to be used for the complex I in-gel activity assay, it was immediately transferred after the run to 5 mM Tris-HCl pH 7.4, 2.5 mg/ml iodonitrotetrazolium chloride (Sigma I8377), and 0.5 mg/ml NADH (Sigma N8129). The gel was incubated at room temperature for 30 minutes, the reaction terminated by addition of 10% acetic acid, rinsed with water and imaged with a GE Amersham Imager. If the native gel was instead used for western blotting, it was rinsed with $ddH_2O$ and transferred to PVDF membrane (Thermo LC2007) using NuPAGE Transfer Buffer and a semi-dry transfer apparatus for 20 minutes at 180 mA (0.18 A). The membrane was then incubated in 8% acetic acid for 5 minutes on a shaker, rinsed with ddH2O, rinsed in methanol for 1 minute, and then transferred to 0.5X TBST for 5 minutes. The membrane could then proceed to blocking and incubation with primary antibodies (see below).

SDS-PAGE western blots were performed with either isolated mitochondria (as above) or with whole worm lysate, prepared by snap-freezing worm pellets of equal volume in liquid nitrogen and then mixing with NuPAGE LDS sample buffer and boiling at 100°C for 20 minutes, followed by centrifugation at maximum speed for 10 minutes. Samples were run in 4-12% NuPAGE Bis-Tris gels for 2 hours at 100 V. Gels were transferred to nitrocellulose membranes using the iBlot Dry Blotting system, and then blocked in 5% milk in TBST for 1 hour. Membranes were incubated in primary antibodies overnight at 4°C in 5% milk/TBST. The following day membranes were washed for 1 hour in TBST, incubated with secondary antibodies (1:10,000 dilution) for 1 hour at room temperature in 5% milk/TBST, and then washed in TBST for another hour. Blots were developed using Pierce ECL Western Blotting Substrate (Fisher 32209) and imaged with a GE Amersham Imager.

For western blots of mouse brains, samples were rapidly harvested, flash-frozen in liquid nitrogen, and pulverized in liquid nitrogen using a mortar and pestle. Total proteins were isolated in RIPA buffer with EDTA-EGTA (Boston Bioproducts) supplemented with EDTA-free COmplete protease inhibitor cocktail (Roche) and quantified using the Pierce BCA protein assay (Thermofisher). 10 μg of total protein extracts in 1X Laemmli SDS-Sample buffer with beta-mercapto ethanol were separated by SDS-page using Novex WedgeWell 4-12% or 14% Tris-Glycine precast gels (Invitrogen) and transferred into polyvinylidene difluoride membranes (Biorad) using the Transblot Turbo blotting system (Biorad). Membranes were blocked in 5% milk in TBST for 1 hour at room temperature and incubated in primary antibodies overnight at 4°C in 3% milk/TBST. The following day membranes were washed for 30 minutes in TBST, incubated with secondary antibodies (1:10,000 dilution) for 1 hour at room temperature, and then washed for 30 min in TBST. Immunodetection was performed according to standard techniques using enhanced chemiluminescence (Western Lighting Plus, Perkin Elmer) captured in Amersham Hyperfilm.

To generate mitochondrial membranes for *in vitro* assays mitochondrial pellets were generated as above (from 10x starting material!) and resuspended in [20 mM Tris- HCl, 1 mM EDTA, 10% glycerol, pH 7.4] and stored at -80°C as described.[66] Mitochondrial suspensions were thawed on ice and sonicated in 1 mL volume in a round bottom 2 mL tube at 10% amplitude (2 seconds on, 1 second off) for 1 minute. Sonicated samples were ultra-centrifuged at 75,000g for 1 hour at 4°C. The pellets containing mitochondrial membranes were homogenized in resuspension buffer and stored at -80°C. All *in vitro* assays at 21% oxygen were performed in a PerkinElmer EnVision Plate Reader at room temperature using absorbance spectrophotometry. NADH oxidation assays were carried out in 10 mM Tris-SO4 (pH 7.4), 250 mM sucrose, 1.5 μM cytochrome c (Sigma C7752), 15 μg/ml alamethicin (Sigma A4665), 25 μg/ml mitochondrial membranes (protein), and 200 μM NADH (Sigma N8129), and consumption of NADH was monitored at 340 nm (minus 380 nm). Amplex red assays were carried out in 10 mM Tris-SO4 (pH 7.4), 250 mM sucrose, 1.5 μM cytochrome c, 15 μg/ml alamethicin, 80 μg/ml mitochondrial membranes (protein), 10 μM NADH, 1 μM or 0 μM piericidin, 2 U/ml HRP (Sigma 516531), 10 U/ml SOD (Sigma S5395), and 10 μM Amplex Red (ThermoFisher A12222) and production of resorufin was monitored at 557 nm (minus 620 nm). *in vitro* assays at 1% oxygen were performed in a Cytation 5 plate reader from Biotek, housed in a hypoxia glove box from Coy Lab Products. Normoxia-matched controls were performed on the same instrument immediately following or preceeding runs in hypoxia.

## Mass spectrometry

Quantitative tandem mass tag proteomics was performed by the Thermo Fisher Center for Multiplexed Proteomics in the Department of Cell Biology at Harvard Medical School. From frozen worm pellets total protein quantification was performed using the micro-BCA assay by Pierce. Samples were reduced with DTT and alkylated with iodoacetimide. Proteins were precipitated using methanol/chloroform and the pellet resuspended in 200 mM EPPS, pH 8.0. Digestion was performed sequentially using LysC (1:50) and Trypsin (1:100) based on protease to protein ratio. Peptides were detected (MS1) in the Orbitrap; sequenced (MS2) in the ion trap; and quantified (MS3) in the Orbitrap. ~2 μl of each TMT-labelled sample was mixed to verify labelling success. Peptides were separated using a gradient of 3 to 27% 90% Acetonitrile in 0.1% formic acid over 180 minutes. MS2 spectra were searched using the Comet algorithm against a custom *C. elegans + E. coli* database containing its reversed complement and known contaminants. Peptide spectral matches were filtered to a 1% false discovery rate (FDR) using the target-decoy strategy combined with linear discriminant analysis. Proteins were quantified only from peptides with a summed SN threshold of >100. Raw data available in Table S3.

To determine the redox potential of the quinone pool, worms were washed in M9 buffer for 30 minutes, rinsed again in M9 to remove *E. coli* contamination, and incubated on ice. The worm pellet was extracted in 1 mL 95% methanol, 5% hexane. Samples were vortexed, bath sonicated for 1 minute, then spun down at 21.1 k x g for 20 minutes. 1 μL of each sample was analyzed using a Q Exactive Plus Orbitrap Mass Spectrometer with a DionexUltiMate 3000 UHPLC system (Thermo Fisher Scientific). Metabolites were separated on a Phenomenex Luna C8(2) column (2 X 30 mm, 3 μM particle size). Mobile phase A was 3% Methanol, 97 % water,

10 mM formic acid. Mobile phase B was 100% methanol with 2mM ammonium formate, and 0.15% formic acid. The gradient was: 90% B for 0-2 minutes, increased to 99% B from 2-8 mins, held at 99% B from 8-12 minutes, decreased to 90% B from 12-12.5 minutes, held at 90% B from 12.5-14 minutes. The flow rate was 300 μL/min. The MS data acquisition was positive ionization full scan mode in a range of 550–2000 m/z, with resolving power of 140,000, AGC target of 3E6, and maximum injection time of 80 msec. All LC-MS data was collected with samples injected in a randomized order. Data was processed with TraceFinder 4.1 software, quantifying the ammonium adducts of $Q_9$ and $Q_9H_2$.

## QUANTIFICATION AND STATISTICAL ANALYSIS

All statistical analyses were performed using GraphPad Prism software. Statistical tests are detailed in the Figure Legends. Typically, statistical significance was calculated using one-way ANOVA followed by correction for multiple hypothesis testing. Error bars represent standard deviation and 'n' refers to the number of animals tested in a single experiment. n.s. = not significant, * = p value <0.05, ** = p value <0.01, *** = p value <0.001.

CellPress
OPEN ACCESS

# Supplemental figures

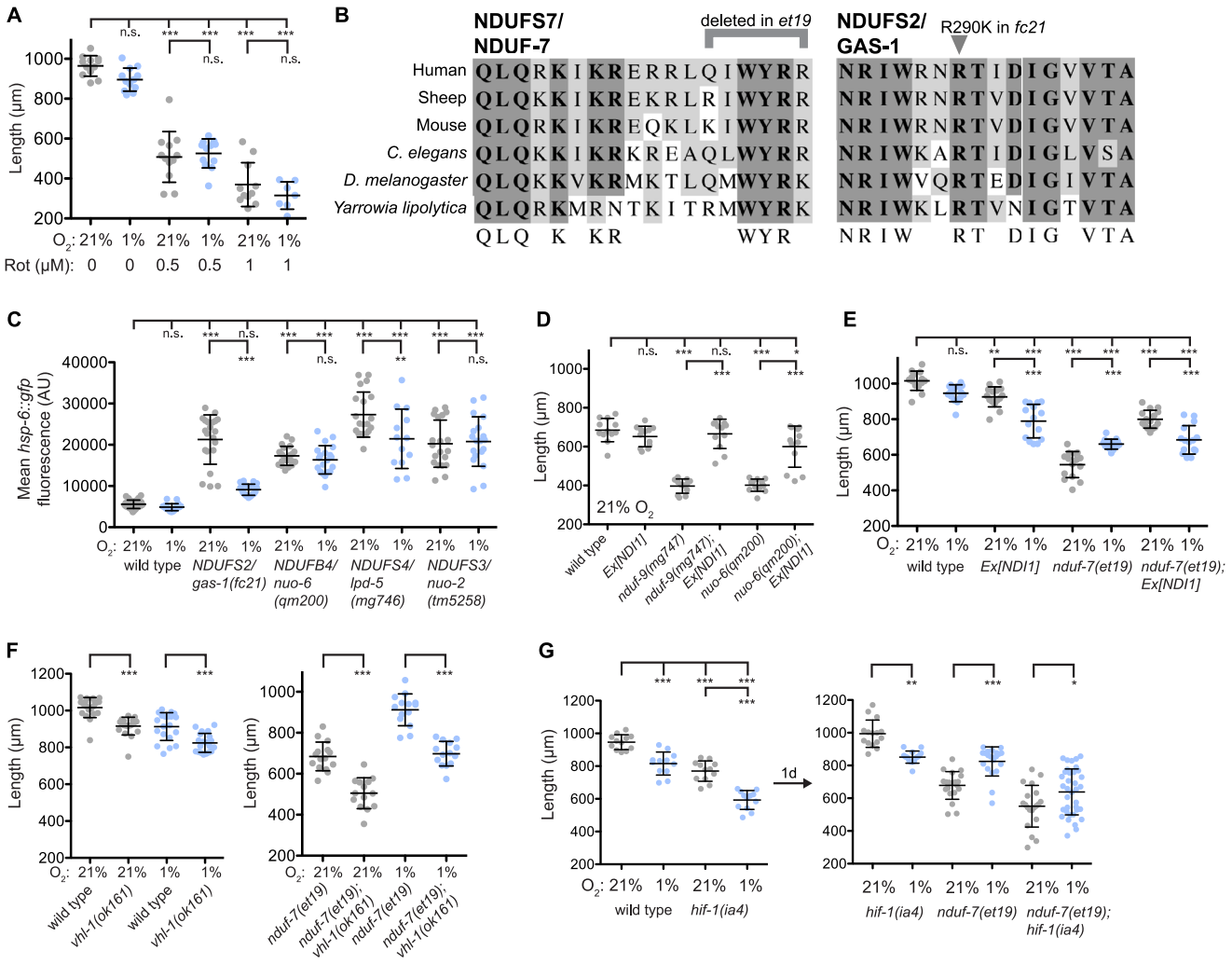


**Figure S1. A subset of complex I mutations are rescued by hypoxia independent of HIF, related to Figure 1**

(A) Growth of wild-type animals for 2 days at room temperature exposed to differing concentrations of the complex I inhibitor rotenone.

(B) Multiple sequence alignment of NDUFS2/GAS-1 (*C. elegans* residues 284–299) and NDUFS7/NDUF-7 (*C. elegans* residues 182–199) including homologs from mammals, invertebrates, and fungi made using ClustalW.

(C) Mean intestinal fluorescence of *hsp-6::gfp* in age-matched animals grown at 21% or 1% oxygen for one generation. All genotypes were imaged at L4/young adult stage except *nuo-2(tm5258)* which arrest at L2 stage.

(D) Growth of animals for 2 days at 20°C.

(E) Growth of animals for 2 days at room temperature.

(F and G) Growth of animals for 2 days (left) and 3 days (right) at room temperature. In all panels, statistical significance was calculated using one-way ANOVA followed by Tukey's multiple comparison test. Error bars represent standard deviation. n.s., not significant, *p value < 0.05, **p value < 0.01, ***p value < 0.001.

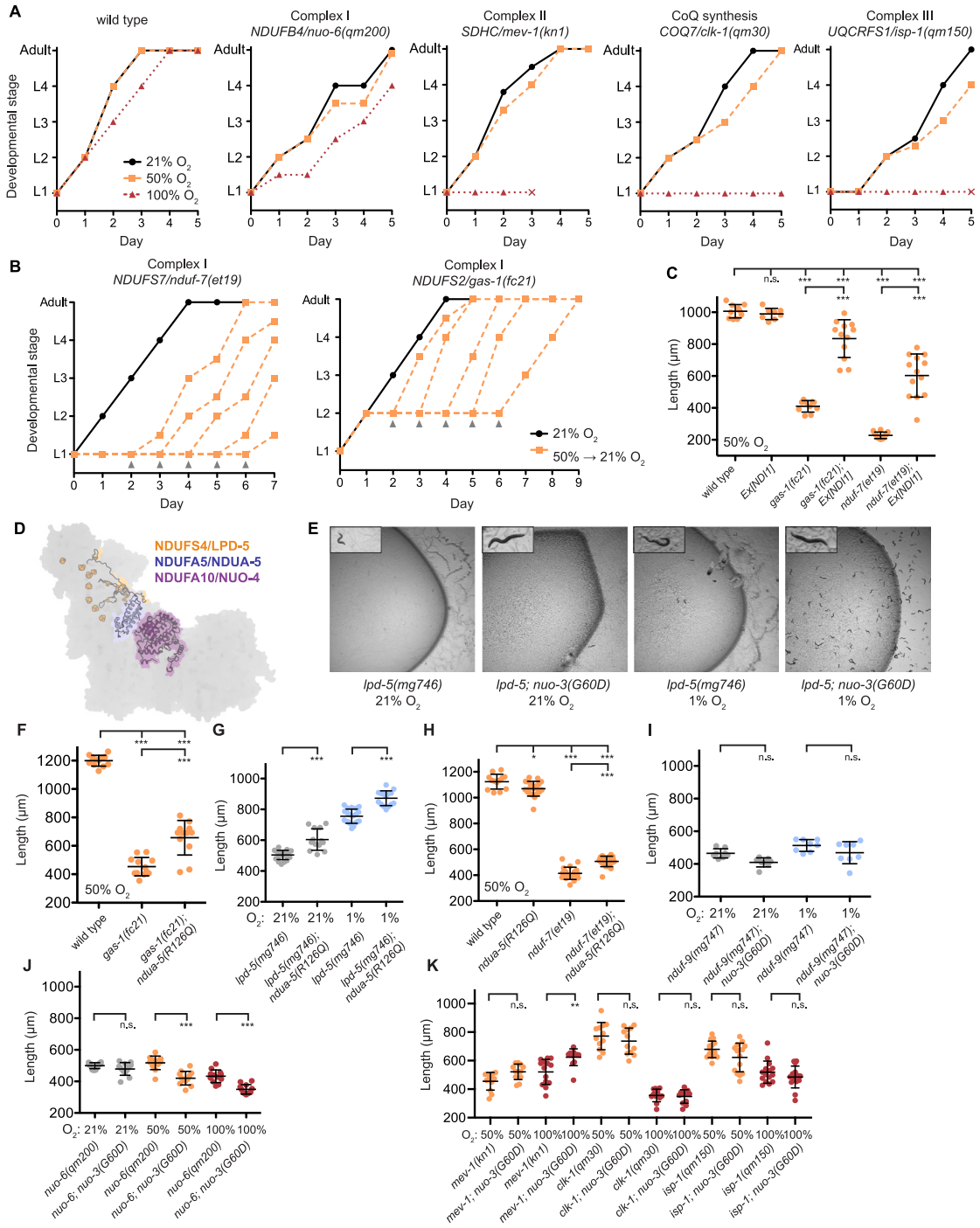


**Figure S2. Complex I mutants rescued by hypoxia are sensitive to moderate hyperoxia and suppressed by intra-complex mutations in *NDUFA6* or *NDUFA5*, related to Figure 2**

(A) Growth of animals following L1 synchronization at 21% oxygen (black), 50% oxygen (orange), or 100% oxygen (red) incubated at 20°C. "x" indicates animals were dead.

(B) Growth of animals following L1 synchronization at 21% oxygen (black) or 50% oxygen for 2–6 days and then shifted to 21% oxygen (orange) at 20°C. Gray arrows indicate the day animals were shifted from 50% to 21% oxygen.

(C) Growth of animals for 3 days at 50% oxygen incubated at 20°C.

(D) Ovine complex I (PDB: 6ZKC[25]) in closed conformation. The NDUFA5/NDUA-5(R126Q) suppressor mutation lies at the interface of NDUFA5 and NDUFA10.

(E) Images of animals after 1 generation growth at 1% or 21% oxygen at room temperature. Magnification = 7×.

(F and G) Growth of animals for 3 days at room temperature.

*(legend continued on next page)*

(H) Growth of animals for 2 days at 50% oxygen followed by 1 day at 21% oxygen.
(I) Growth of animals for 5 days at room temperature.
(J) Growth of animals for 2 days at room temperature.
(K) Growth of animals at 50% oxygen for 4 days at room temperature, or growth at 100% oxygen for 2 days followed by 21% oxygen for 2 days at room temperature. For all panels, statistical significance was calculated using one-way ANOVA followed by Tukey's multiple comparison test. Error bars represent standard deviation. n.s., not significant, *p value < 0.05, **p value < 0.01, ***p value < 0.001.

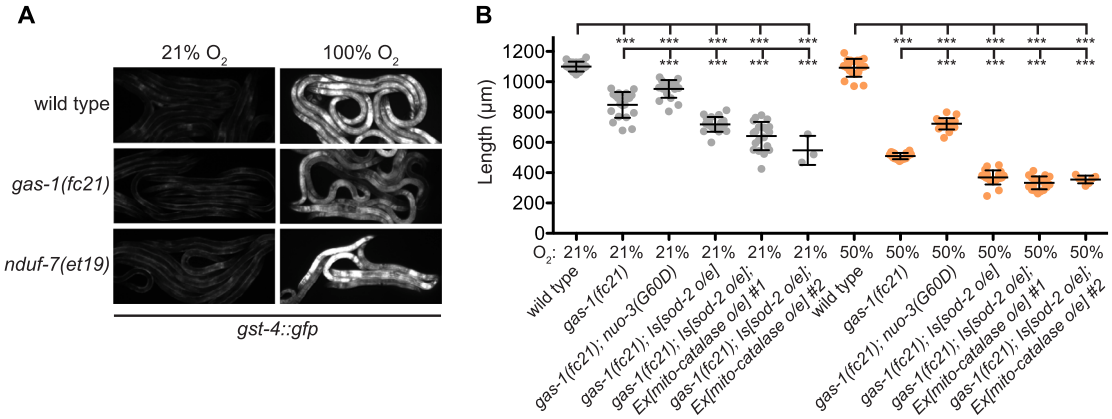


**Figure S3. Rescue of complex I mutants by hypoxia and *nuo-3(G60D)* is not due to alleviation of mitochondrial ROS toxicity, related to Figure 3**

(A) Fluorescent images of L4 stage animals containing *gst-4::gfp* grown continuously at 21% oxygen or exposed to 100% oxygen for 1 day. Images were acquired at 69× magnification with an exposure time of 50 ms.

(B) Growth of animals for 3 days at 20°C at 21% or 50% oxygen. Statistical significance was calculated using one-way ANOVA followed by Tukey's multiple comparison test. Error bars represent standard deviation. ***p value < 0.001.

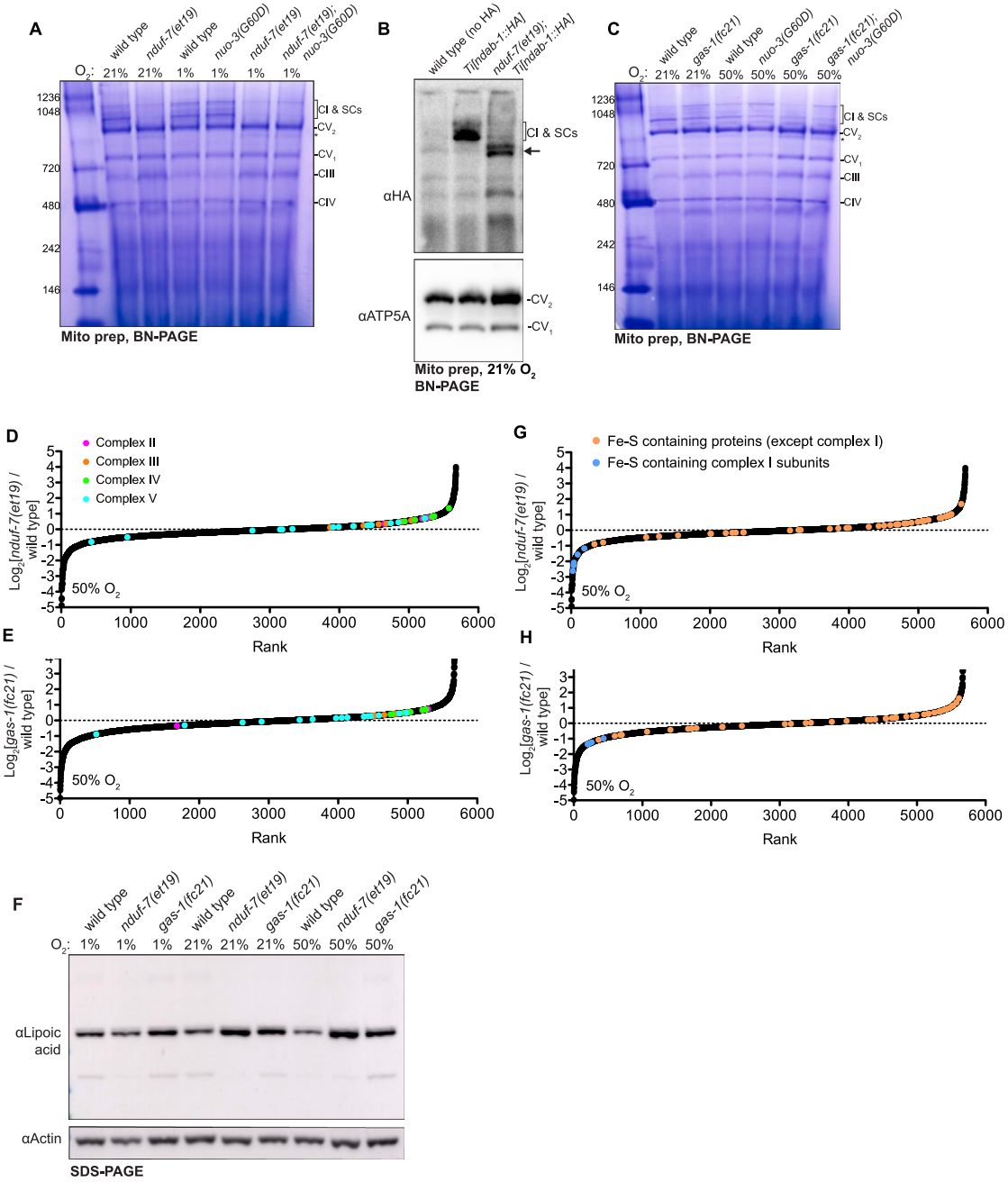


**Figure S4. Complex I levels are compromised in oxygen-sensitive mutants, but their restoration does not underlie the rescue by hypoxia or *nuo-3(G60D)*, related to Figure 4**

(A) Blue native PAGE of isolated mitochondria purified from animals grown at 21% or 1% oxygen for 4 days. * denotes faint band that may correspond to CI subcomplex.

(B) BN-PAGE of isolated mitochondria followed by western blot from animals grown continuously at 21% oxygen. Black arrow indicates CI subcomplexes observed in *nduf-7(et19)*, which run at the same size as complex V dimers.

(C) BN-PAGE of isolated mitochondria purified from animals grown at 21% or 50% oxygen for 2 days.

(D and E) TMT quantitative proteomics from animals exposed to 50% oxygen for 2 days. Plotted are log 2-fold ratios of all proteins from which at least two peptides were quantified.

(F) SDS-PAGE of whole worm lysate from animals exposed to 21% or 50% oxygen. Anti-lipoic acid antibodies recognize the modified E2 subunits of PDH (DLAT) and OGDH/KGDH (DLST).

(G and H) TMT quantitative proteomics from animals exposed to 50% oxygen for 2 days. Plotted are log 2-fold ratios of all proteins from which at least two peptides were quantified. Iron-sulfur cluster containing *C. elegans* proteins were identified by homology to a previously published list.[67]

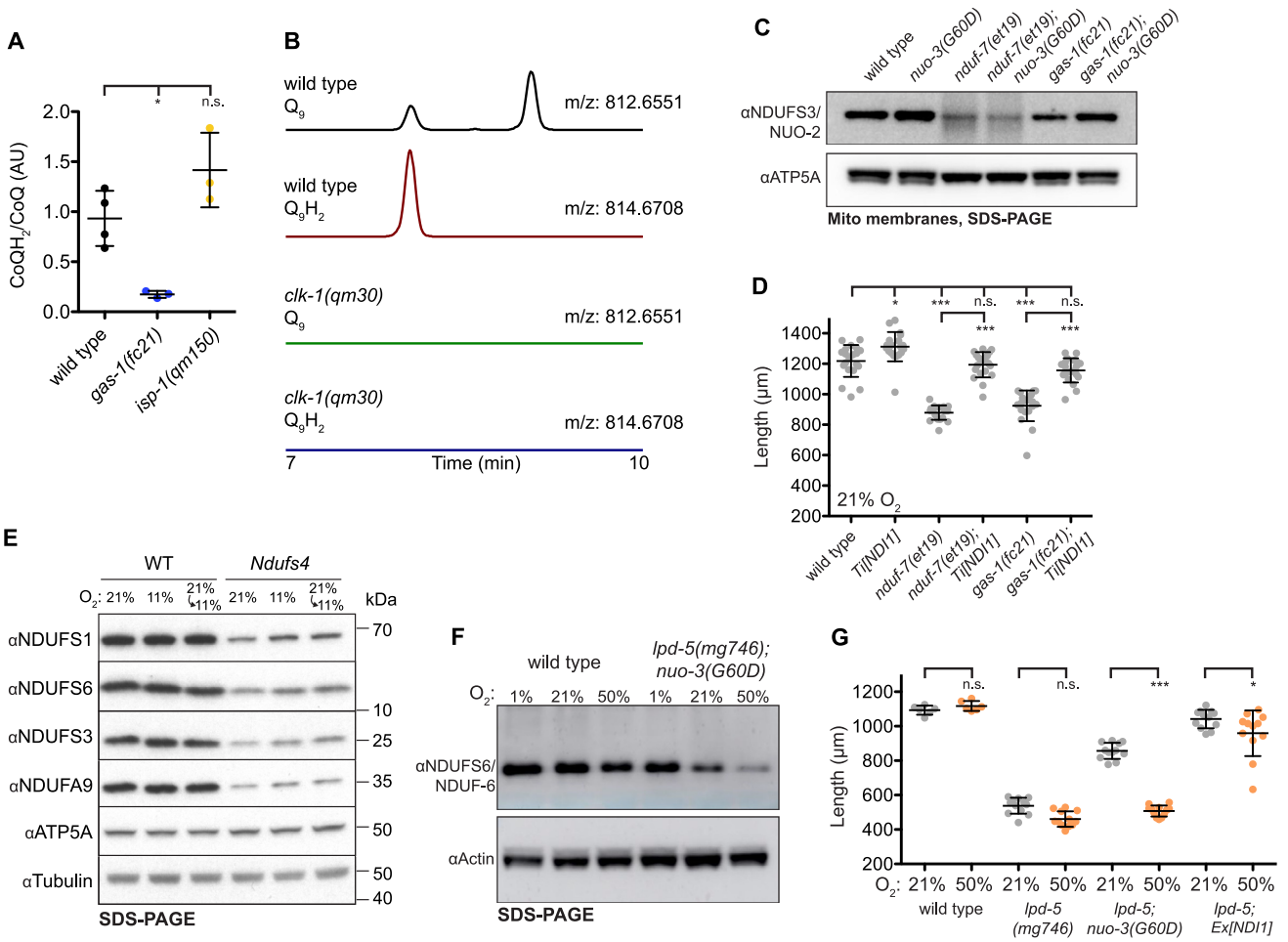


**Figure S5. *NDUFA6/nuo-3(G60D)* and hypoxia rescue complex I forward activity in oxygen-sensitive mutants, related to Figure 5**

(A) Ratio of reduced $CoQ_9H_2$ to oxidized $CoQ_9$ as determined by mass spectrometry. Samples were extracted from whole worms grown continuously at 21% oxygen.

(B) Mass spectrometry traces of $CoQ_9H_2$ and $CoQ_9$ in wild-type and *clk-1(qm30)* backgrounds. *clk-1* mutants can survive using dietary $CoQ_8$ from their bacterial food.

(C) SDS-PAGE followed by western blot of *C. elegans* mitochondrial membranes used in *in vitro* assays.

(D) Growth of animals for 3 days at room temperature at 21% oxygen.

(E) SDS-PAGE followed by western blot of brains from wild-type or *Ndufs4* mice exposed to 21% oxygen, 11% oxygen from weaning (days 25–30), or shifted from 21% to 11% oxygen after 55 days.

(F) SDS-PAGE followed by western blot of whole worm lysate from animals grown continuously at 1% oxygen and then exposed to 1%, 21%, or 50% oxygen for 3 days.

(G) Growth of animals for 3 days at room temperature. For all panels, statistical significance was calculated using one-way ANOVA followed by Tukey's multiple comparison test. Error bars represent standard deviation. n.s., not significant, *p value < 0.05, **p value < 0.01, ***p value < 0.001.

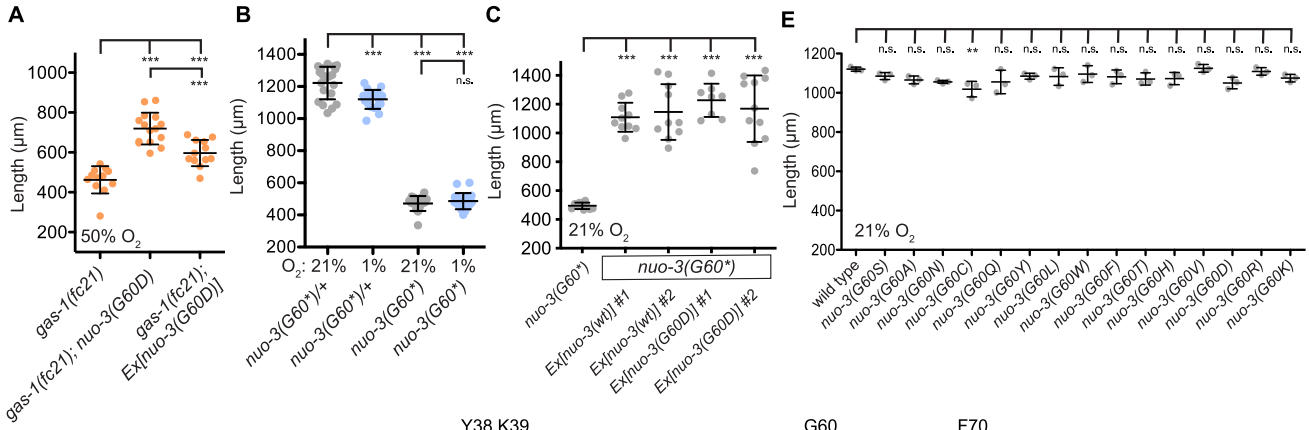


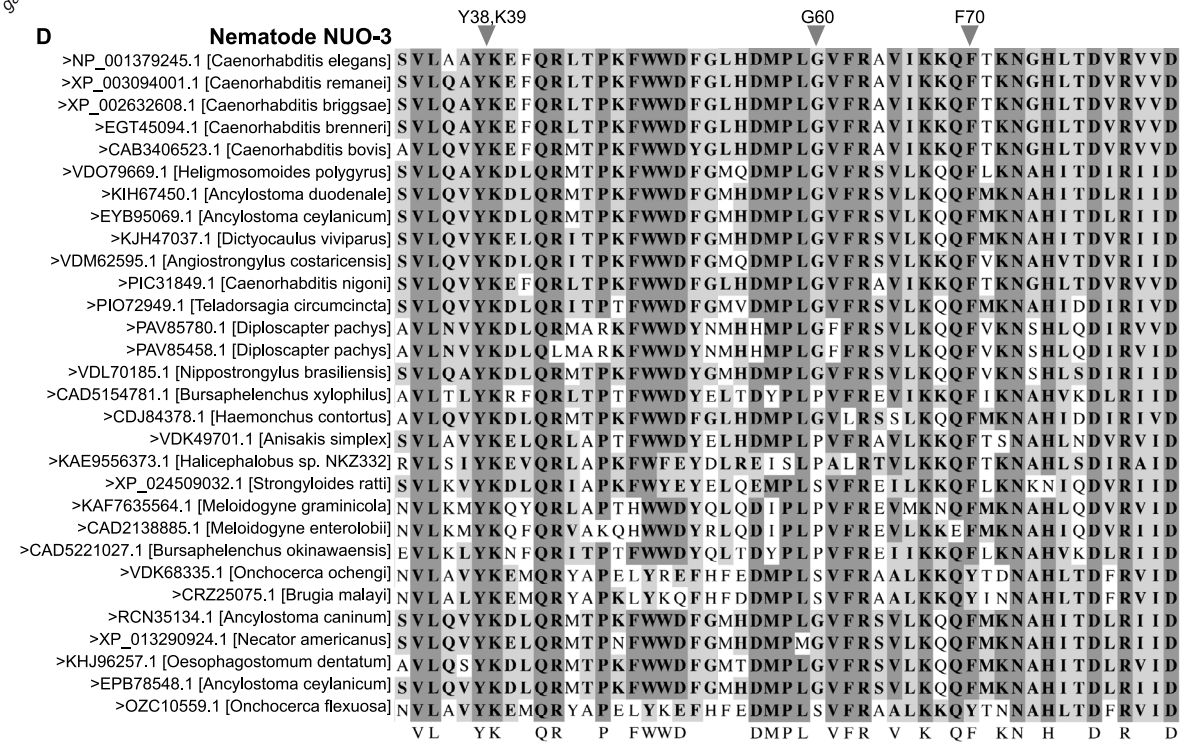


**Figure S6. Complex I rescue by *NDUFA6/nuo-3(G60D)* requires LYRM domain activity, related to Figure 6**

(A) Growth of animals for 4 days at 50% oxygen.

(B) Growth of animals for 3 days at 21% or 1% oxygen at room temperature.

(C) Growth of animals for 4 days at 21% oxygen at 20°C.

(D) Multiple sequence alignment of NDUFA6/NUO-3 homologs from nematodes (above) and eukaryotes (below) made using ClustalW. The alignment corresponds to amino acids 33–83 of *C. elegans* NUO-3.

(E) Growth of animals for 3 days at 21% oxygen. For all panels, statistical significance was calculated using one-way ANOVA followed by Tukey's multiple comparison test or Dunnett's multiple comparison test (E). Error bars represent standard deviation. n.s., not significant, *p value < 0.05, **p value < 0.01, ***p value < 0.001.

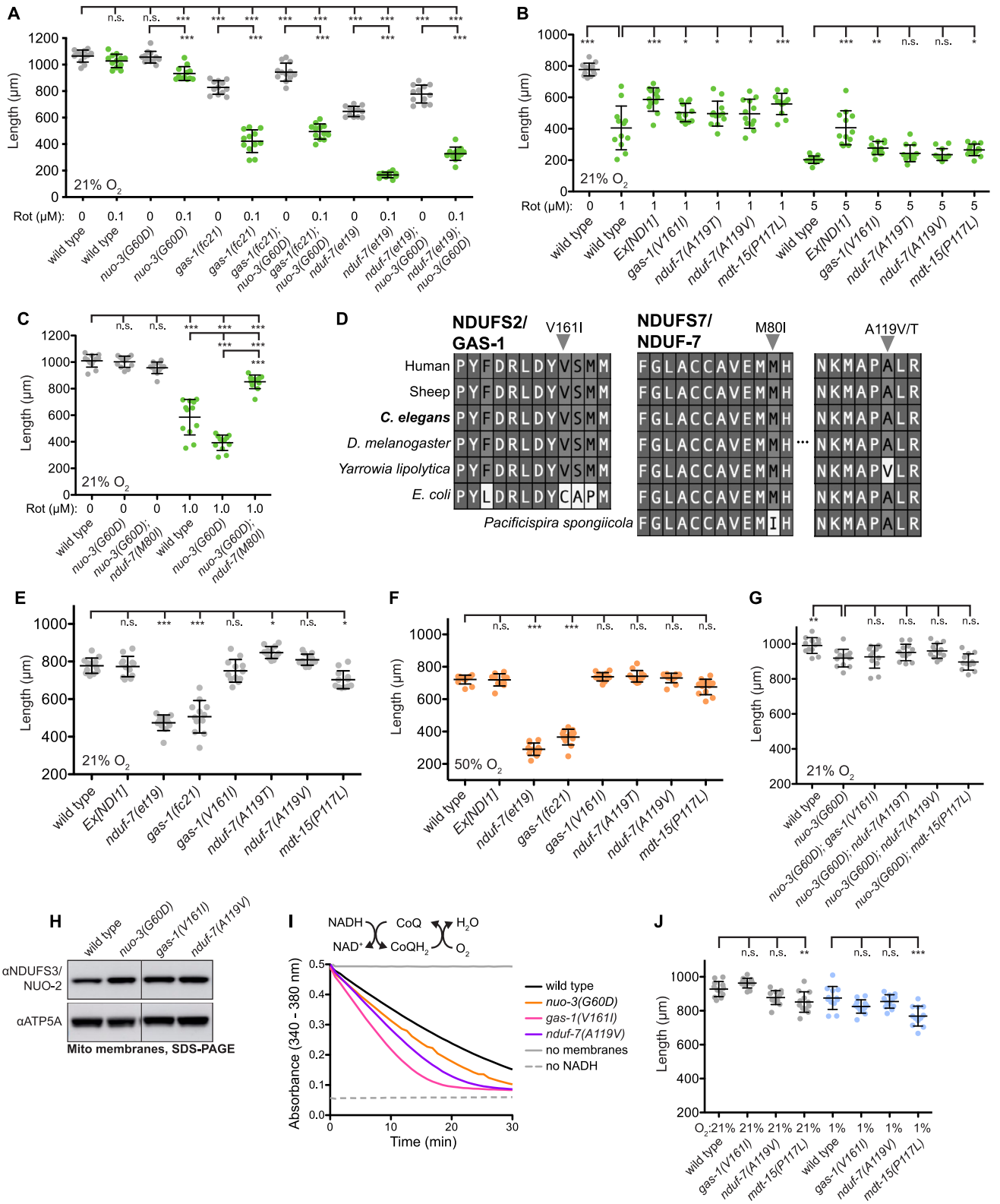


*(legend on next page)*

**Figure S7. Mutations surrounding the CoQ binding pocket block the ability of *NDUFA6/nuo-3(G60D)* or hypoxia to rescue complex I, related to Figure 7**

(A) Growth of animals for 3 days at 21% oxygen with 0 or 0.1 μM rotenone.
(B) Growth of animals for 2 days at 21% oxygen with 0, 1.0, or 5.0 μM rotenone incubated at 20°C.
(C) Growth of animals for 2 days at 21% oxygen incubated at room temperature with 0 or 1.0 μM rotenone.
(D) Multiple sequence alignment of NDUFS2/GAS-1 (*C. elegans* residues 153–164) and NDUFS7/NDUF-7 (*C. elegans* residues 70–81…114–121) including homologs from animals, fungi, and bacteria made using ClustalW.
(E) Growth of animals for 2 days at 21% oxygen incubated at 20°C.
(F) Growth of animals for 2 days at 50% oxygen incubated at 20°C.
(G) Growth of animals for 2 days at 21% oxygen incubated at room temperature.
(H) SDS-PAGE followed by western blot of *C. elegans* mitochondrial membranes used in *in vitro* assays.
(I) Complex I-dependent oxidation of NADH by isolated mitochondrial membranes at 21% oxygen. NADH absorbs light at 340 nm.
(J) Growth of animals for 2 days at 21% or 1% oxygen incubated at room temperature. For all panels, statistical significance was calculated using one-way ANOVA followed by Tukey's multiple comparison test (A, D–F, and H) or Dunnett's multiple comparison test (B). Error bars represent standard deviation. n.s., not significant, *p value < 0.05, **p value < 0.01, ***p value < 0.001.